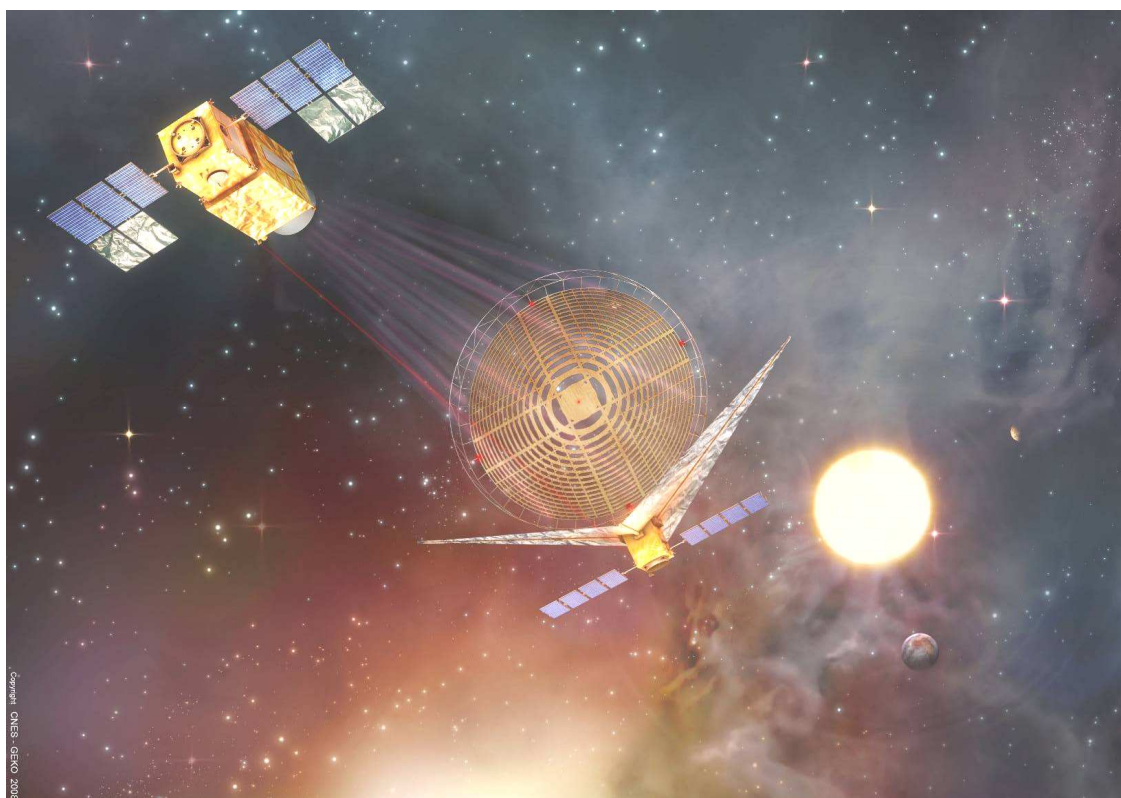# Very high resolution
Fresnel Diffractive Array Imager
for the Ultraviolet

ESA Cosmic Vision 2015-2025 plan

Proposal for a Medium-size mission

03/12/2010

Laurent Koechlin (1),

Marco Delbo (3),
Ana Ines Gomez de Castro (4),
Matthiew Hayes (7),
Margarita Karovska (5),
Daniel Kunth (6),
William J. Merline (8),
Roser Pello (1),
Jean-Pierre Rivet (3),
Paolo Tanga (3)

Paul Deba (1),
Paul Duchon (2),

(1) Observatoire Midi-Pyrénées / IRAP /
Signal Image Instrumentation
14 avenue Edouard Belin
31400 Toulouse, FRANCE

(2) 16 avenue du Mont Frouzi
31810 Venerque, FRANCE
at CNES (from 1970 to 2008)

(3) Observatoire de la Côte d'Azur
 Boulevard de l'Observatoire
 B.P. 4229 F-06304 NICE Cedex 4, FRANCE

(4) Fac. de CC Matematicas
Universidad Complutense de Madrid
28040 Madrid, SPAIN

(5) Harvard Smithsonian Center for Astrophysics (CfA)
60 Garden St.
Cambridge Ma 02138, USA

(6) Institut d'Astrophysique de Paris (IAP)
UMR7095 CNRS, Université Pierre & Marie Curie,
98 bis boulevard Arago,
75014 Paris, FRANCE

(7) Observatoire de Genève
51 ch. des Maillettes
CH-1290 Versoix
SWITZERLAND

(8) Southwest Research Institute
1050 Walnut St. #300
Boulder, CO 80302 USA

1. Executive Summary

1.1 Goals

The Fresnel Diffractive Array Imager (FDAI) will explore three themes in Cosmic Vision: "From gas and dust to stars and planets", "Asteroids and other small bodies", and "The evolving violent Universe". These themes will be addressed by image and spectral data in the ultraviolet domain, with 0.01 arcsec angular resolution and very high contrast capabilities.

The Ultraviolet domain is yet unexplored at the high resolution and dynamic range that will be reached by a Fresnel imager. It will address:

- High-energy phenomena around AGN and compact galaxies: the UV emission of galaxies is a clue to star formation. This is also a very rich source of information for astrochemistry, on a very high number of spectral lines.

- Exoplanet formation around young stars: planetary systems form within circumstrellar dust disks can be studied in the UV. At resolutions of 0.007" it will also study the shape, short time-scale evolution and chemical reactions that occur between the dust grains and the gas, triggered by the stellar radiation.

- Spectral imaging of small and large solar system objects: more than 1000 solar system objects closer than a few astronomical units can be mapped at a 0.01" resolution. Statistics on binary asteroids with small companions will yield shapes, masses, densities, and spectra. Atmospheres and vicinity of planets will be probed at high contrast.

1.2 Optical principle involved

A large and lightweight aperture (the Fresnel Array) collects light, and focuses it on a secondary spacecraft, 15 to 20 kilometres downstream. In this two spacecraft formation-flying mission, the primary spacecraft holds the focusing element: a light-weight membrane; the secondary spacecraft is placed at focus and holds the focal instrumentation. The positioning tolerances are large: in the millimetre range for translation in the image plane, and approximately one metre for inter-spacecraft distance.

The Fresnel Array is a thin membrane, 4 x 4 meter square. It is opaque, but punched with specially shaped holes (subapertures), which cover close to 50% of its surface. This layout focuses light by diffraction and forms a direct image. No other large optical element is required. Light travels entirely in a vacuum, from the entrance of the instrument to the primary image plane. The consequence is a potentially very broad wavelength domain, and a very pure wavefront leading to high contrast and diffraction limited images at all wavelengths.

Pupil plane

Image plane
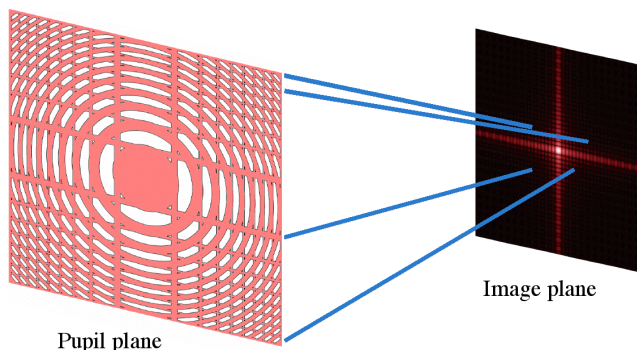
Fig 1.2-1: Image of a point source (Point Spread Function) given by a Fresnel Array. The four spikes around the bright central lobe have a low relative luminosity (10^{-3}), they are amplified, to be visible in this display. The four quadrants delimited by the spikes have a very low residual background level (10^{-6} to 10^{-8}).

1.3 Features

– The angular resolution of a Fresnel Array is equal to that of a solid aperture having the same size. It increases as the wavelength shortens. It reaches 6.2 milliarcseconds at 121 nm wavelength with a 4-m aperture.

– The image quality is restricted by the precision at which subapertures are carved and positioned in the Fresnel Array. This manufacturing constraint is loose compared to optical surfacing: a $\lambda/25$ wavefront, required for high dynamic range, is obtained with a ~0.1 millimeter precision in the plane of the array. The required planarity of the membrane for a $\lambda/25$ wavefront, is in the order of a centimetre. These tolerances are independent of wavelength.

– The Fresnel Array casts light at focus into a central peak flanked by four orthogonal spikes, rather than diffraction rings occurring with circular apertures, or broad side lobes with interferometric arrays. Most of the image field of a Fresnel Array is at high "rejection rate".

– Fresnel Arrays act as transmission gratings: only 6 to 7% of the incident light is focused, the rest being either blocked by the opaque parts, or diffracted into other orders, not focused, and finally blocked by ad hoc optical layout in the focal instrumentation. As a consequence, a 3 to 4-fold increase in size is required to collect the same number of light as a solid aperture. The comparison in terms of image brightness depends if the object is extended or unresolved. However, comparison with filled apertures should be made in terms of cost rather than size.

– The inherent chromaticity of diffraction focussing is corrected after prime focus by small size diffractive or dispersive optical elements in a pupil plane: a secondary Fresnel grating, blazed to optimize transmission. The resulting correction is complete and independent of the wavelength. However, for a given inter-spacecraft distance, the bandwidth is limited to $\Delta\lambda/\lambda \sim 20\%$ due to the size of the field optics at focus that collects the beam in the primary image plane. With two wavelength channels, we propose to cover the UV region from $\lambda = 117$ nm to 190 nm. Light will be fed into one channel at a time by changing the attitude of the Receiver Spacecraft, and the inter-spacecraft distance adjusted accordingly.

– Long focal lengths are implied for this 4-meter Fresnel Array: 15.7 to 20.1 km, at respectively $\lambda \approx 170$ nm and $\lambda \approx 133$ nm, therefore requiring formation flying in a low gravity gradient region of space such as L2.

1.4   State of the art

The Fresnel Array concept has now been tested for over five years: we have designed and built a 19-meter focal length breadboard, qualified on sky targets at *Observatoire de Nice* (France).


Fig 1.4-1: *200 mm aperture, 18-meter focal length Fresnel primary array placed at the front end of a19-meter refractor tube for validation on sky sources. (696 Fresnel zones ,~250 000 subapertures).*
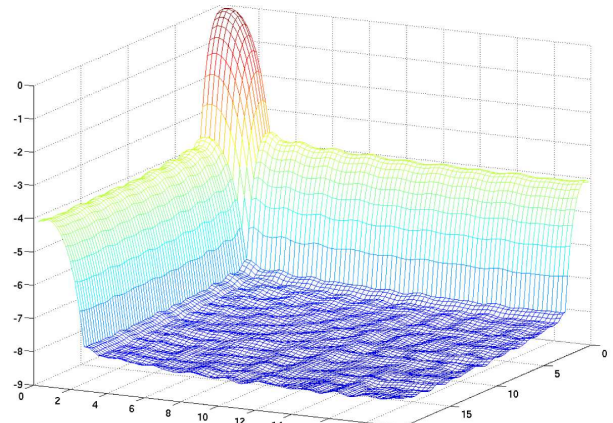
Fig 1.4-2: *Simulated quarter field PSF of an apodized 600 zone Fresnel Array. Vertical axis: log normalized brightness. Horizontal plane: position in the field (resels). The dynamic range is close to 10^8.*

We have validated the chromatism correction scheme on artificial sources (500nm < λ < 750nm), and on sky sources (650nm < λ < 900nm). The image quality is diffraction limited, and the best dynamic range reached on the sky is 6.2 10^{-6} for the satellites of Mars. Our testbed also allowed validating numerical simulation software for large Fresnel Arrays. These simulations yield a dynamic range (rejection factor) close to 10^{-8} for arrays such as the 4 m one we propose here. At long exposure times, a dynamic range of 10^{-8} allows detection at contrasts of 10^{-9}, the limiting factor being the variance of the noise. In one of our publications [Koechlin 2005] we present simulations of exoplanet study, but this will be limited to large planets and there are many other science cases, for a 4-m aperture.
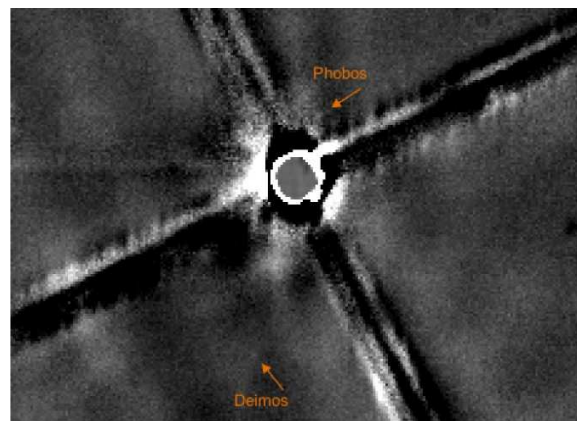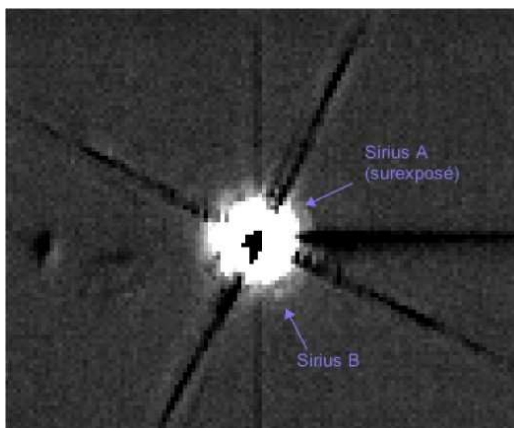
Fig 1.4-3: Images of binary star Sirius AB (left) and satellites of Mars (right) made with our 20-cm aperture Fresnel imager testbed, during the validation phase of diffraction focusing from the ground, in the visible and close IR (650-900 nm band). To our knowledge, no image of the satellites of Mars had been made before with optics as small as 20 cm.

The UV domain is not the only one where FDAI can be used: at larger apertures (10 to 30 m) their diffraction limited imaging capabilities can be competitive also in the visible and IR. If this membrane technology is validated at 4-meter scale, it may open the way to much larger apertures in space, and telluric planet study.

2. Introduction

In 2020-2025, the UV domain will have been covered by COS on the HST, and presumably by WSO-UV: a 1.7-m, wide field UV telescope to be launched in 2014. The Fresnel imager, if launched, will operate in the same spectral domain after these previous UV spacecrafts have completed their mission. So, what will it bring more?

It will have a much higher angular resolution and dynamic range. It will peek into the close environment of bright sources, being able to catch very faint phenomena in transition regions. This will address science cases in three Cosmic Vision themes:

- From gas and dust to stars and planets,
- Asteroids and other small bodies, and
- The evolving violent Universe.

The science cases we propose will be detailed in the "scientific objectives" section. First, we describe shortly the instrument, as it has large differences compared to classical telescopes.

This proposed 4-meter "Fresnel Diffractive Array Imager" (FDAI) is a two spacecraft Formation-Flying (FF) telescope. The tolerances in positioning fit well within the capabilities of present technology: for example in the order of 1 metre for the inter-spacecraft distance set at a few kilometres.

The rationale of this proposal is to make competitive science in the UV with a "medium size" 4-meter aperture, and also to open the way for future large space observatories that would use this diffraction focussing technology, where it can be an alternative at all wavelengths to large classical space telescopes and to interferometry.

High dynamic range imaging in the UV is difficult because optical surface roughness at small scale causes scattering. In addition, the angular resolution is rarely diffraction limited because of surface imprecision at large scale. The Fresnel imager removes these problems. Its optical concept forms an image with light that has travelled entirely in vacuum on its way to prime focus. This allows high dynamic range and diffraction-limited images at any wavelength. In the proposed configuration, the angular resolution is that of a 4x4 meters square aperture: 0.007 arc seconds at λ=121 nm.

The FDAI also has drawbacks, such as the need to correct chromatism, some bandwidth and field limitation, and a low (<10%) transmission. However, this does not hamper its capabilities for the science cases described further.

For example, with a 20 cm aperture testbed in the 750-900 nm waveband, we obtained images of the satellites of Mars, Phobos and Deimos. This validation made from the ground is not relevant to the UV science cases we propose, although solar system science is one of the themes. This validation was made to prove the high contrast capabilities on real sky sources, and that a Fresnel imager compares honourably with classical optics. Indeed, as far as we know, the satellites of Mars had never been imaged with such a small aperture.

The 6.8% efficiency in transmission that we achieved in our tests (lab and sky), if applied to a 4 m Fresnel Array, corresponds to having the collecting area of a mirror 1.71 m in diameter, taking into account the square shape of the FDAI, a 80% efficiency for the classical comparison UV mirror coating, and a central obscuration of 0.28 in diameter for the classical comparison telescope. The equivalent collecting area, taking into account the focal instrumentation optics for imaging, is between 5000 and 6000 cm^2. This leads to a collecting area equivalent to WSO-UV, but with a far better angular resolution.

The deployment technology is also currently under validation, and the opaque membrane material has been studied, one possible solution being kapton covered with a 1 μm thick layer of metal. The thermal and mechanical constraints are described in the "payload" section.

3. Scientific objectives and requirements

Three Cosmic Vision themes will be addressed: "From gas and dust to stars and planets", "Asteroids and other small bodies", and "The evolving violent Universe". More specifically, we propose to study:

- The UV emission in galaxies.
- Exoplanetary systems formation.
- Small and large objects of the solar system.

These domains will be reviewed in sections 3.2, 3.3, and 3.4.

3.1 performance requirements and spectral bands

Using a formation-flying instrument is quite different from a standard space telescope. Steering a 2-spacecraft configuration uses propellant; the total number of individual fields observable during a 5-years mission is limited. This limit depends on the propellant embarked, on the inter-spacecraft distance, and on the speed at which one wants to shift from one configuration to the next. The present proposal is budgeted with a hydrazine reserve of 500 m/s dedicated to science reconfigurations. The total number of different fields observable during a 5-years mission will be between **10000** and **13500**, depending on the observation procedures and wavelengths. Each field will cover a radius of 7 to 12 arc seconds, depending on wavelength. With that, a 5-years mission would for example give internal densities of between 500 and 750 binary asteroid systems.

In order to cover the proposed science cases, we plan to use two (possibly three) spectral bands in the UV. Each spectral band will have its own dedicated focal instrumentation. The relative bandwidths of each will be limited to $\Delta\lambda/\lambda$=25%. This limit comes from the 68 cm diameter of the "field telescope", placed in the receiver spacecraft. For a given position of the receiver spacecraft, at non-nominal wavelengths the beam is defocused. Chromatic correction solves the problem for the light that the 68 cm field telescope can capture, so the defocused beam should not exceed this diameter.

For large wavelength coverage, one has either to use a wider field telescope, or select spectral bands and observe them sequentially. The number of different wavebands has an impact on budget, as changing them requires resetting the inter-spacecraft distance and uses propellant. Each band has its own chromatic correction optics and detectors, optimized for its central wavelength. In this proposal we have budgeted the focal instrumentation optics for two bands, although we had computed the total weight and propellant budget for three bands in the CNES study, in case future collaboration allows.

The wavebands need not be adjacent, and their choice depends on the science cases. The 118-148 nm band containing Lyman-α at 121.5 nm is a very rich for galactic physics at low Z. It is also a rich source of data for the star forming regions, which feature a high number of spectral lines. This band allows the highest angular resolution on stellar photospheres, chromospheres and circumstellar environments, where protoplanetary systems form. However, for the study of solar system objects (except self-luminous phenomena in planetary atmospheres), at longer wavelengths the Sun provides a better illumination and higher limiting magnitude. We propose covering the 118-232 nm, or the 148-285 nm domains with 3 bands.

For the protoplanetary dust discs and forming planetary systems, covering 118-148 nm domain with 2 bands only, would allow to collect data from the Ly-α (121 nm), C IV (155 nm) and OIII (166 nm) lines emitted and/or absorbed in stellar photospheres and close stellar environments. The 0.007 arc second angular resolution would show details at scales of the earth orbit (1 AU) in young star regions at 150 parsecs, and 3 AU at 500 parsecs. The high dynamic range would allow peeking close to bright sources.

The following concerns focal instrumentation, not included in the proposal pricing. The focal instrumentation will be built by member states. Negotiations are pending for possible collaborations with countries participating to the network for ultraviolet astronomy (NUVA).

The focal instrumentation in each band will comprise both imaging and spectral channels. The imaging will be achieved with 2000x2000 or higher resolution photon counting UV cameras. Spectral channels with $R \approx 5 \times 10^4$, and $R \approx 2500$, such as in WSO-UV, will be used.

We plan a compound spectral-imager in the focal instrumentation, combining 1-D-spectral and 2-D-spatial resolution. The optical concept in MUSE, presently built for the VLT, would be downscaled and simplified to fit in a lightweight space instrumentation, providing spatio-spectral coverage of protoplanetary discs.

UV detectors allow long exposure times as their background noise is very low: 3×10^{-4} count /s /pixel in Near UV, and 4.10^{-5} count /s /pixel in far UV. Their quantum efficiency is for the moment around 30%, but recent UV

detector technologies promise efficiencies close to 60% available commercially in Europe.

The images and spectra will be computed on-board from the photon coordinates data. Depending on targets and science requirements, the exposure times will extend from a few minutes for bright sources up to several hours for high dynamic range or faint objects. The total exposure time on a given field is planned to be between 6000 and 8000 s. These figures come from an optimisation of the number of fields attainable during 5 years mission, considering the propellant reserve.

3.2 The Lyman alpha universe

Many energetic and compact objects in galaxies are present at $Z < 2$ (including ours). They are a clue to galaxy evolution and structure, and one of the first links that allow understanding of the distant universe.

Lyman-α is a cosmic line copiously produced by ionized hydrogen, the most abundant species of the Universe. For this reason, and because of its rest frame wavelength at 121.6 nm, it remains potentially a remarkable tracer of star formation from the local to the most distant universe. However, due to its resonant nature, Lyman-α photons undergo multiple scatterings within the HI gas because they can escape and eventually reach the observer.

Local galaxies have been for many years the ideal sites to investigate the many parameters that govern the transfer mechanisms and control the visibility of the Lyman-α line. In particular it has been found that unlike what had been anticipated in early investigations performed with the IUE, the dust itself is not the primary factor that controls the Lyman-α escape. In other words it has been found that galaxies with relatively large dust content could be strong Lyman-α emitters while nearly dust-free galaxies would reveal a pure damped Lyman-α absorption line. Owing to the HST-GHRS and HST-STIS spectroscopy, the role of the kinematics of the gas has revealed to be a crucial for letting Lyman-α escape at velocities where the HII gas is not affecting these photons anymore. Finally further deep Lyman-α images performed with the ACS have shown scattered Lyman-α photons forming extended diffuse component extending far from the source and comprising 90% of the total Lyman-α flux.

Combined with studies performed at high Z with other telescopes we now can make appropriate corrections and produce interesting cosmological implication such as the evolution of the Lyman-α escape fraction with time and establish the fraction of galaxies that are missed by Lyman-α techniques. But since Lyman-α is now a routinely used technique for the finding of distant galaxies it remains crucial to pin down the characteristics of Lyman-α emitters if we wish to interpret the distant Universe.

Although we have a better grasp on the Lyman-α processes in the ISM, we still admit that given the many parameters at work we still have no ways to quantify their relative importance. One of the reasons is a lack of large number of known local emitters that could span these many parameters, hence the difficulty to make them correspond to distant LAEs. From this point of view, UV FDAI could be a very important imager capability that would allow us to assess the importance of the scattering process in close-by, but also distant galaxies that are seen with nearly no spatial resolution from ground based telescope and even with HST.

3.2.1 Metal content of galaxies and chemical enrichment process

It is possible that some local dwarf galaxies in the nearby Universe still contain pristine gas (Kunth & Sargent 1986; Kunth et al.1994). The role of the neutral gas upon the chemical evolution of galaxies is twofold. First, it acts as a massive reservoir for the molecular hydrogen which fuels star-formation.

The dispersion spatial and time scales as well as the mixing time scale are however relatively unknown in galaxies and dwarf galaxies in particular.

Few BCDs for which the comparison was made between chemical abundances in the HI envelope and in the ionized gas of their HII regions includes the 2 lowest-metallicity star-forming galaxies known IZw18 (Aloisi et al. 2003; Lecavelier et al. (2004) and SBS0335-052 (Thuan al.2005) and more metal rich ones such as IZw36 (Lebouteiller et al.2004), and Pox36 (Lebouteiller et al.2009). Fundamental results can be drawn from these studies: (1) the abundances in the neutral gas show that this phase has been already enriched in heavy elements, and (2) the abundances in the neutral gas are systematically equal or lower than those in the ionised gas. These results suggest that the neutral envelope of BCDs appears to be less chemically evolved than the ionised gas associated with the current star-formation episode. Data also indicate an apparent threshold of 1/50 Zo in the neutral gas of BCDs. All these results of importance rest on the hypothesis that we master the problem of saturated lines. This is a difficult point that can only be solved observationally providing that lines of very low oscillator strengths can be observed with enough spectral resolution (10000). Also spatial information will help to identify one single line of sight with only one UV source (namely an O star) as a background and with little or no contamination. In this sense, the UV FDAI can play an important role (over existing data gathered with COS and WSO) with its larger collecting area (to look for fainter and fainter lines), and its excellent spatial resolution.
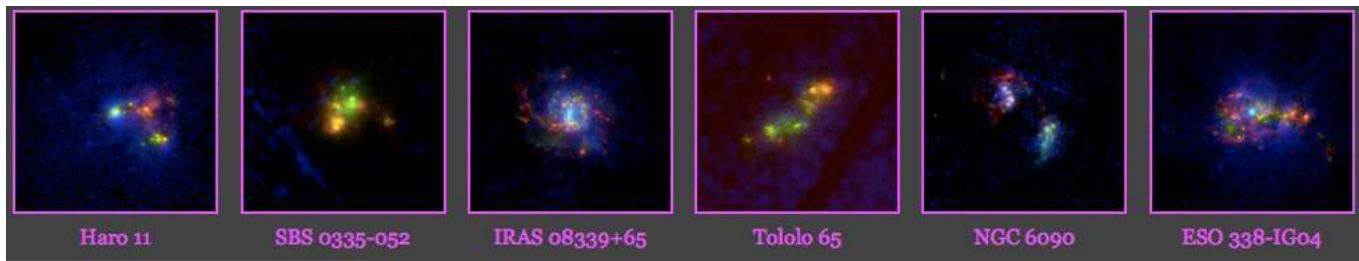
Fig 3.2-1 *HST images in three bands: two UV bands + Hα, by H. ATEK, D.Kunth, M.Hayes et al. The sensitivity of FDAI will be similar or higher, but its 0.007 arc second resolution will allow to resolve at least 5 times more precisely the structure of these galaxies.*

3.2.2 WR galaxies

Episodes of star formation are fascinating events in the Universe, characterised by the presence of hot stars and ionised gas. In giant HII regions, clusters of young stars produce ionising photons and winds that largely impact the surrounding medium. They are strong UV emitters and produce lines of characteristics P-Cyg profiles. These regions are naturally very crowded and difficult to study without enough spatial resolution. Moreover the evolution of these clusters strongly depends on metallicity (affecting their wind dependance) requiring to investigate galaxies of different metal content, hence different distances. WR stars are short-lived phase of these O stars from which they descend. For this reason the study of the WR/O ratio calls to their metallicity dependance and the process of star formation (mode and age) in a given galaxy. It is a well-known fact that models up to now fail to reproduce this ratio (Brinchmann et al, 2008). A thorough study of the most representative WR local galaxies would enlighten this problem. UV FDAI would be able to obtain the WR/O ratio from star counts after isolating WR stars using appropriate filters from the O population.

3.2.3 The Lymann continuum and the source of re-ionisation

We know little about the sources of re-ionisation of the Universe. Many hypotheses are advocated i.e. from QSOs, to starburst galaxies, but no clear convincing answer has been proposed so far. There have been some measure of the Lycont leakage from star burst galaxies using the FUSE on a very small sample of redshifted star burst galaxies so as to place the Lyman limit in the 92 nm to 100 nm range. UV FDAI would open a new opportunity.

3.2.4 Lyman-Continuum leakage at low and intermediate redshifts

By necessity, galaxies at redshifts beyond 7 must have emitted a substantial fraction of their ionising photons in order to drive the reionisation of the Universe (e.g. Bouwens+2009; Bunker+2010). The escape fraction of these photons still remains a vital but missing parameter in all the cosmological radiative transport simulations of reionisation (e.g. Iliev+). Unfortunately, due to the rapidly increasing density neutral gas clouds in the IGM, ionising wavelengths will never be observationally accessible at redshifts beyond 4 (Inoue & Iwata 2008), and thus in order to empirically test the leakage of ionising radiation, lower-redshift analogues samples are required. FDAI's imaging capabilities make it the ideal instrument through which to search for LyC leakage from starburst galaxies at redshifts of ~1 (FUV channel) and >~1.5 (NUV). Furthermore, recent observations (Iwata+2009) have shown that at z~3, galaxies that do emit LyC radiation show an unexpected spatial offset from the restframe UV (tracing massive stars), although Vanzella+(2010) have suggested that this effect may be due to interloper contamination at lower redshifts that cannot be disentangled at ground-based (~1 arcsec) resolutions. Thus space-based UV imaging telescopes are essential to examine the LyC leakage problem in star-forming galaxies, and also operate at the required resolutions for geometrical test.

3.2.5 Lyman-α galaxy astrophysics

The Ly-alpha emission line has repeatedly proven itself to be an invaluable tool by which to identify star-forming galaxies at the highest redshifts (Hu&Cowie1998; Rhoads+2001; van Breukelen 2005; Venemans+2005; Nilsson+2007; Hibon+2010; Hayes+2010. Unfortunately, being a resonance line, the interpretation of these survey data remains far from straightforward (Neufeld 1990; Verhamme+2006), and empirical calibrations / transport studies are a necessity. From this perspective, galaxies in the distant Universe are typically too faint to study at the requisite S/N and vital supplementary information is redshifted to inaccessible wavelengths. Again, samples of nearby analogue galaxies are needed. This has been done with HST/GHRS (Kunth+1998) and STIS (Thuan&Izotov 1997; Mas-Hesse+2003) but due to extreme HST pressures, only upon small, handpicked, and biased samples. The R=2000 spectroscopic mode of FDAI offers an opportunity to obtain large samples of spectroscopic samples of local galaxies in Ly-alpha, sufficient to resolve the line profile and study the inferred

kinematic properties. This is basically the only method by which we can empirically study the necessary transport physics in the most cosmologically important emission line feature.

3.2.6 Helium II reionization and the helium Ly-α forest

Using the R~50 000 spectroscopic mode, we can very precisely measure the He II Ly-alpha forest against bright background QSOs at redhshifts between 3 and 5; the redshift at which the origin of the H I ionising background is thought to be shared between star-forming objects and AGN. Comparing this against the optically derived HI LAF from the same QSOs provides a direct model-independent assessment of the two species in a huge number of individual absorbing systems. Thus comparison of the forests gives an unbiased measurement of the hardness of the ionising background and its fluctuations (Miralde-Escude 1993), measurements of the underlying temperature and density of the IGM (Furlanetto&Lidz 2010), and the overall average evolution with redshift. Tests have previously been done at lower redshifts with FUSE (Zheng+2004; Fechner&Reimers+2007; Worseck+2007), although the small aperture limited the number of sightlines on which it was possible. Remarkable improvement has recently been offered with HST/COS (Shull+2010), however many sight lines are required in order to analyse the effects of the relatively rare hard ionising sources (intervening QSOs) for proximity studies.

3.3 Stars, planetary systems and accretion astrophysics

How do protostellar disks evolve into planets? Which is the role of UV radiation in the photoprocessing of disk material ? Do jets contribute to modify disk properties and evolution? To what extent does multiplicity affect disk structure ? These are but a few of the unanswered questions concerning young planetary disks evolution.

Accretion is one of the most powerful mechanisms for generating energy in the Universe, in sources ranging from Young Stellar Objects (YSOs), planet forming environments, to interacting systems such as wind accreting binaries and Active Galactic Nuclei) AGN.

High-angular resolution imaging studies of the environments of these sources using FDAI and a set of UV lines (eg. C|V, Mg II h&k) will provide unprecedented insights into the physical mechanisms of accretion and its impact on shaping the environment in many galactic and extragalactic sources.

3.3.1 Disks around pre-main sequence (PMS) stars

Though spectroscopic studies have provided much information on the chemical composition of disks, there are still many unsolved questions that require imaging and spectral imaging, with very high spatial resolution, to be answered. A basic scheme of the structure of Solar-System precursors, i.e. T Tauri Stars (TTSs), is outlined in [Fig.3.3-1]. The spectral ranges where the bulk of the energy of each component is radiated are indicated. The dusty atmosphere of the disk partially, scatters the radiation from the innermost region and partially absorbs it and photoprocess it. Radiation from the star (optical to UV) is absorbed by the disk and re-emitted in the infrared together with the internal disk radiation produced by the accretion driven disk heating. As a result, the thin atmosphere and halo of protostellar disks can only be studied at short wavelengths since the contrast with the disk thermal emission is the largest. Fortunately, the best-studied protostellar disks are orbiting around powerful UV sources.

A 4-m probe to FDAIs technology, tuned to UV wavelengths will provide fundamental information on disk physics and evolution. As today, most of the interfometric imaging of pre-main sequence stars have been done on Herbig Ae/Be (HAeBe) stars since they are the most luminous of their kind, having lasting disk structures. The existence of inner dust walls and dust-devoided inner regions in protostellar disks has been unveiled from the observations of these sources. The peak of emissivity of HAeBe stars is in the ultraviolet. The fact that dust grains in protostellar disks are larger than in the InterStellar Medium (ISM) also favours the propagation of UV photons to large distances. Observing some few HAeBe with a 4-m UV FDAI probe will provide unvaluable information on young planetary disk evolution and the role of photoevaporation on gas phase removal from protostellar disks.
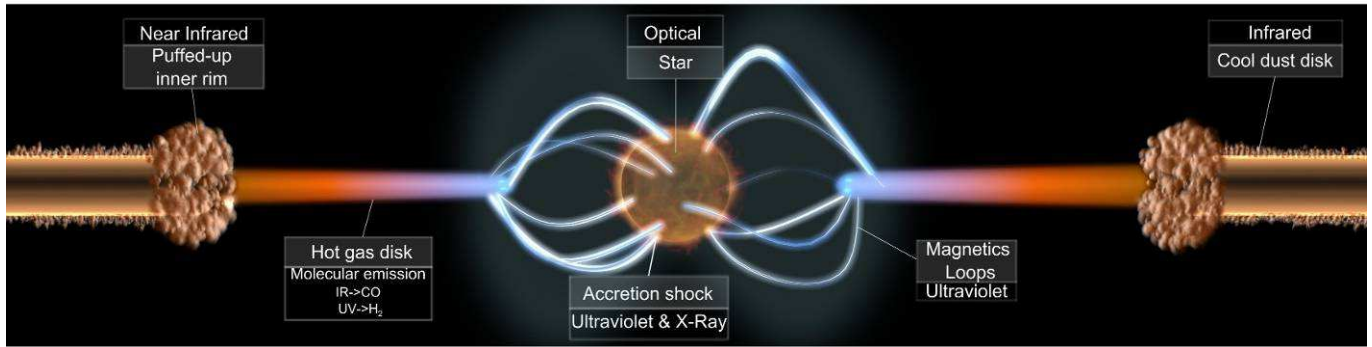
<u>Fig 3.3-1</u>: *Sketch of the inner structure of T Tauri Star disk. The spectral ranges where the bulk of the energy of each component is radiated are indicated. The inner border of the disk is the boundary with the stellar magnetosphere. Another important boundary is set by the dust melting point that separates the two thermal regimes of the disk: gas dominated versus dust dominated.*

The nearest star forming regions are in a ring of radius ~150 pc around the Sun. This ring marks the molecular walls of the Local Bubble in the ISM and forms part of a local kinematic and physical structure in the Galaxy known as the Gould's Belt. Thus, this distance defines the target angular resolution for disks studies: 7 mas to resolve 1 AU scales or 0.07 mas to resolve the boundary between the star and the disk. Currently, the only way to achieve such a high resolution is by means of interferometry at optical and infrared wavelengths. Typical facilities have baselines of about 100 m and probe wavelengths of 1-13 microns providing spatial resolutions of 2-10 mas or 0.25-1.25AU. These wavelengths trace hot dust emission (300-1800 K) from the disk inner AU. As shown in [Fig.3.3-2], ground based interferometry (optical to radio wavelenghts) trace the large scale structure of the disk but no the innermost region where the gravitational field is stronger and the stellar irradiation etches the disk surface. FDIAs are fundamental to cover this fundamental area of the discovery space not only for disks studies but also for understanding the formation of jets and collimated outflows.

Infrared interferometric maps of HAeBe stars have shown disks as extended ellipses due to the projection of the circular disk on the plane of the sky. At 1 - 4 µm, disc emission is expected to be dominated by hot dust at the disc surface that scatters the stellar radiation. In fact, there is a strong correlation between the measured disc radii (r) and the luminosity of the central stars (L_{star} / r) proportional to $L_{star}^{1/2}$ (Millan-Gabet et al 2007). The observed discs radii are too large for the inefficient grazing incidence illumination of the disc surface. Direct illumination by the star is required instead, i.e., an inner disc cavity devoid of dust must exist around the star. Measured radii are consistent with the dust sublimation radii of relatively large dust grains (1µm) with sublimation temperatures in the range 1000K-1500K. The existence of this dust sublimation ring has been independently inferred from the bump in the near infrared energy distribution of Herbig stars (Natta et al 2001). The inner rim of the disc is expected to be puffed-up by hydrostatic equilibrium but its vertical structure is still unclear. The inner cavity of the disc is filled in with hot gas that is well traced by the CO fundamental (Δv =1) ro-vibrational transition at 2.3 µm. However, this inner cavity is heavily irradiated by the stellar UV photons that pump the electronic transitions of the most abundant molecules (H_2, CO...) that are also observed at UV wavelengths. The spectral energy distribution of HAeBe stars (pre-main sequence stars with masses of 2-10 solar masses) and the low mass T Tauri stars (< 2 solar masses) is shown in [Fig.3.3-3]; both of them are powerful UV sources.
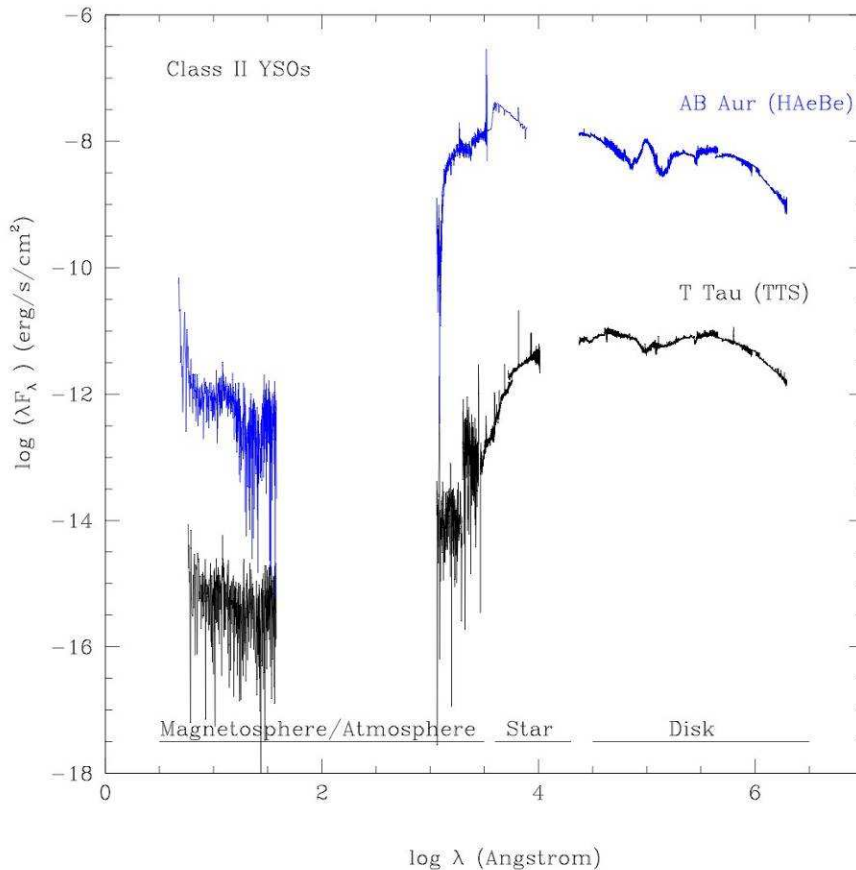
Fig 3.3-2: *Spectral energy distribution of T~Tau, a TTS (in black) and AB~Aur and HAeBe stars (in blue). The main contributors to the flux in each spectral range are marked at the bottom. T~Tau flux is reduced by two orders of magnitude (-2 in the Y-axis scale) to avoid confusions. AB~Aur and T~Tau are prototypes of their classes.*

In summary: FDIAs are ideally suited to map the inner AUs of protostellar discs around HAeBe stars and to study disc photoevoration and the creation of inner puffed up disc borders. Spectro imaging with FDAIs will allow to track the stellar variability and the presence of screening objects in the light path (from clusters of small bodies, to dusty plumes and irregular puffed up inner holes). Some of the brightest and nearest TTSs (such as TW~Hya or AB~Dor) could be also studied with the 4-m generation FDAIs. This UV information is strongly needed to interpret the flow of data that will come from the large facilities working at other frequencies such as ALMA or Optical interferometers to study protoplanetary and young planetary disc (Millan-Gabet et al 2007). Modest (4-m) FDAIs will be instrumental to cover the evolutionary gap from disc photoevaporation to planet formation (see Alexander et al 2004). UV imaging at scales below 10 milliarcseconds will provide unique information on the gas component of the inner disc, on the interaction between gas, dust and the photoionizing UV radiation in young planetary discs. These data are *needed* for the physical modelling of the coupling between gravitational and magnetic stresses on the protostellar discs (as well as for the related chemical modelling). The α-prescription is used to describe angular momentum transport and heating in discs. The name of the prescription comes from the α parameter used to scale the stress with the local pressure. In spite of its success to model the discs spectral energy distribution, it is still unclear why the α prescription works in protostellar discs. The disc conductivity has to be high enough, to allow the Magneto Rotational Instability (MRI) to set in and feed the turbulence cascade that permits mass transport. However, the penetration of photoionizing radiation and particles to the disc midplane is not enough and there seems to be a dead region where only dynamos working on the dusty disc atmosphere could permit transport (Gammie, 1996). To measure the degree of irradiation and the properties of the disc atmospheric gas/dust is fundamental for this purpose.

FDIAs will also allow to address the study of the influence of binarity on disc evolution; reaching spatial scales below 10~AUs is strongly required for this purpose. Some few selected sources could be imaged during the rotation period; there are about ten pre-main sequence close binaries known within 140 pc and some of them are powerful UV emitters like Ak Sco (Gomez de Castro 2009). Tracking PMS binaries with highly eccentric orbits will also allow to study the evolution of the inner disc and orbit circularization (i.e. Hanawa et al 2010).
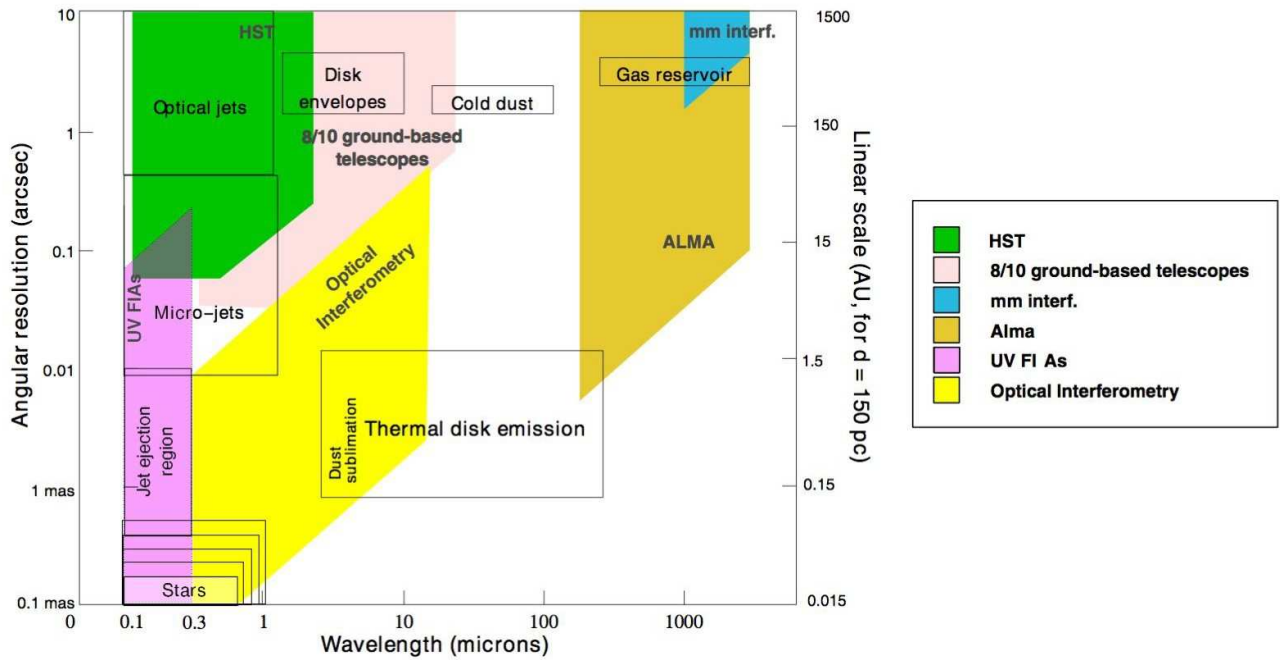
Fig 3.3-3: *In this Wavelength-Resolution diagram we plot the domains covered by different instruments (colour trapeziums), and the domains where different science cases reside. One can see that the UV FDAI imager covers a region that was not observable before.*

3.3.2 High-energy winds and symbiotic stars

Models of accreting interacting systems show a complex morphology in the close circumbinary or circumnuclear environments, including structures in a form of spiral waves and collimated outflows/winds and jets. These structures are usually overwhelmed by the brightness of the central source(s). However, the regions surrounding the central engine of many interacting systems will become clearly "visible" once the emission from the bright components is significantly suppressed using the FI powerful imaging capabilities.

Hydrodynamical models of wind accretion show that the mass transfer through a focused wind could be a common mechanism for a broad range of wind interacting systems, many potential targets for the FDAI. One example of these are the symbiotic systems and their close circumbinary environments. Symbiotic systems are fascinating accreting binaries with a key evolutionary importance since they are potential progenitors of a fraction of Planetary Nebulae and of SN type Ia. A typical symbiotic consists of a mass-losing AGB or a red giant star and a hot accreting companion, often a white dwarf, and sometimes even a neutron star. The components are assumed to be detached (not filling their Roche lobes, at least during most of the orbital motion) and the companion accretes mass from the wind of the cool evolved star.

Hydrodynamical models [eg. de val Borro et al. 2009] show that even in semi-detached and detached binaries (like symbiotic systems) with evolved mass losing star, there can be a Roche lobe overflow (RLOF)-like accretion via a stream flow (as detected in the X-ray and UV images of the wide separation symbiotic Mira AB - [Karovska et al. 2005]). The "focused wind" accretion rates can rise up to 10% of the mass loss from the primary. These accretion rates are an order of magnitude higher than the accretion rates predicted by the simple Bondi-Hoyle wind accretion calculations.

The FDAI will be able to image in detail the regions surrounding the components of these systems as shaped by the focused wind accretion and the winds from the individual components.
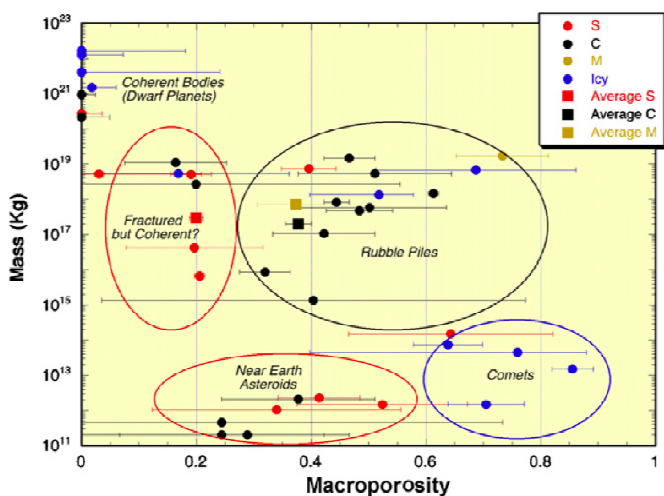
3.4 Solar system objects

FDAI will allow us to measure the bulk density of asteroids in a size and distance range that have never been accessed before. Even though an angular resolution of 0.01 arc second is achievable from the ground with AO, there are two main differences when using a Fresnel imager: the stability of images, and the streilh ratio quasi equal to 1 at all wavelengths.

The density and internal structures, among the most important characteristics of asteroids, are also some of the least constrained, and they will continue to be so in the future. When compared with the densities of meteorites - a partial sample of the building blocks of asteroids that survive the passage through the Earth's atmosphere - one can deduce the nature of asteroid interiors. These physical properties of asteroids reflect the accretional and collisional environment of the early solar system. Moreover, because asteroids are analogs to the building blocks that formed

the terrestrial planets 4.56 Gy ago, the density and internal structures of minor bodies inform us about the formation conditions and evolution processes of planets and the solar system as a whole.

It is worth to note that, at the time of writing, the orbits of more than 500,000 asteroids are known; in the next future sizes and geometric albedos in the visible band (the average surface reflectivity) of more than 150,000 of these bodies will become available, thanks to the measurements obtained with the NASA satellite WISE – that almost completed its mission - and the Spitzer Space telescope. Sizes are crucial to derive the size frequency distribution (SFD) of asteroids, and subpopulation thereof such as dynamical families. SFDs inform us about how 4 Gyears of collisions have shaped the asteroids and about the strength of asteroids and their resistance to catastrophic disruptions. The albedo of an asteroid is strongly related to the surface mineralogy. Thus, the distribution of this parameter amongst asteroids tells us a lot about their origin and composition: e.g. albedo values < 0.10 is an indication of a body with carbonaceous composition. However, for higher albedos (e.g. >0.15) inferring asteroid composition from albedo is a non-unique process. This degeneracy can be broken when the wavelength dependent albedo is known. This information can be obtained from the geometric visible albedo and the reflectance, the latter obtained from spectroscopic observations of asteroids in the visible and/or near infrared. It turns out that the ESA mission Gaia (to be launched end of 2012) will obtain spectroscopic observations of more than 200,000 asteroids at more than 50 epochs over 5 years. Gaia and WISE data combined together will provide a detailed mineralogical/compositional map of the different asteroid populations.
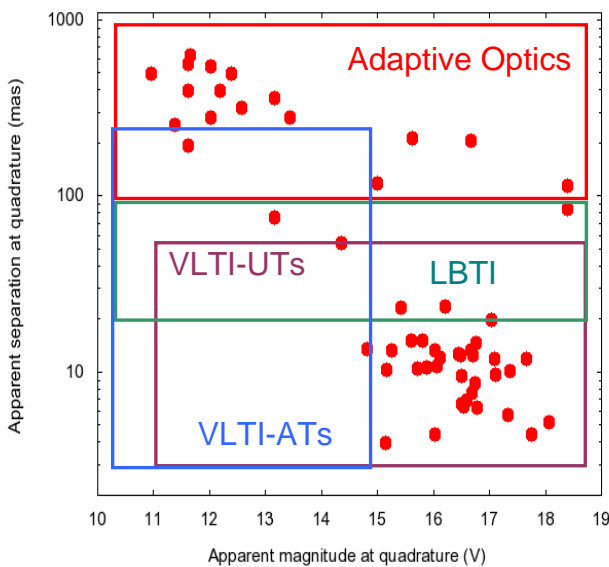
However, these measurements will only inform us about the *surfaces* of these bodies and do not constrain their *interior*. Densities and internal composition are, and will remain, much less well constrained observationally (Fig. 1).

The determination of the bulk density of an asteroid requires knowledge of its mass and volume. There are four robust methods to determine the mass of an asteroid: (1) asteroid–spacecraft perturbations; (2) asteroid–asteroid perturbations; (3) asteroid–planet perturbations; and (4) observations of the motion of asteroid satellites. The first method is by far the most accurate, but is constrained to the rare instances of a close spacecraft encounter. The second method, tracking the motions of asteroids that gravitationally interact with one another, requires modeling the orbits of multiple asteroids over long periods of time and high accuracy astrometry. The best data are for the largest asteroids (1) Ceres, (2) Pallas, and (4) Vesta. It is expected that Gaia will enable us to derive the masses of the largest 100 asteroids (Mouret et al. 2007). For the third method, we note that the largest asteroids Ceres, Pallas, and Vesta can produce measurable perturbations on the motion of Mars. Like the 2nd method, this technique is limited to the largest asteroids.

Fig 3.4.1: *Best knowledge of asteroid macroporosity and internal structure (from Consolmagno et al. 2009). The limit of adaptive optics at 10m class telescopes is > ~10^{17} Kg. This project aims at investigating masses in the range $10^{17} – 10^{14}$ Kg. Note the huge error bars affecting macroporosity determinations.*

Thanks to the high spatial resolution, high sensitivity of FDAI, we can use **the fourth method**, namely the observation of asteroid satellites. This is by far the most productive method and, in principle, not biased towards large objects. This method can provide accurate masses of asteroids since, by Kepler's third law, the orbital period and semimajor axis of the satellite uniquely determine the mass of the system. The best observations yield errors of only a few percent in mass (Merline et al., 2002). The challenge is to determine the semimajor axis of the system, and in general this requires spatially resolving the secondary from the primary. The population of known binary asteroids now exceeds 160, with over 170 known satellites, some of which reside in triple and even one quadruple system (Johnston, 2008 & refs. therein). Asteroids with satellites have now been found in every major dynamical group: near-Earth asteroids (NEAs), Main Belt asteroids (MBAs), Jupiter Trojans, Centaurs and trans-Neptunian objects (TNOs). Statistical studies of the occurrence of asteroid satellites indicate that ~15% of the asteroids with size <20km have a satellite. Up to now, kilometer-sized binary (or triple) asteroids have been studied by radar (Ostro et al. 2006). However, radar is limited to NEAs during favorably close approaches with Earth since the signal-to-noise-ratio of radar observations scales with r^{-4}, where r is the asteroid-radar distance. In the other dynamical populations, binaries have been discovered through direct imaging using adaptive optics on 8 and 10m class telescopes (VLT, Keck) or using the HST (with its superior resolution in space). However, this technique is

limited to well-separated (>100 mas) binaries involving large (>100 km) bodies. Several of these large bodies have been characterized (e.g. Marchis et al., 2003, 2005a, 2005b, 2006a, 2006b; Descamps et al., 2008, 2007a, 2007b). These objects show a remarkable range of orbital and physical characteristics: orbital periods between 0.5 to 80 days, secondary-to-primary size ratios between 0.1 and 1, and asteroid bulk density between 0.7 and 3.5 g/cm^3, which <u>highlight the potential of the study of binary asteroids for the analysis of the internal structure of asteroids.</u>

However, there is another population of binaries, which is discovered by means of photometric lightcurves: this method was proven to be very efficient in the discovery of binary asteroids revealing the presence of the satellite from eclipses. In principle, their density can be derived from extensive lightcurve observations over a large range of solar phase angle and several epochs. However, severe difficulties arise in the case of MBAs, which are observable over a relatively moderate range of phase angle (Scheirich et al., 2008 and Scheirich and Pravec, 2009): see Fig. 2. Typically, binary asteroids discovered through lightcurves are too small to be characterized with direct imaging and too distant for radar. High-angular-resolution observations (<100 mas) are thus critical for the characterization of small and distant binaries in the Main Belt.

Fig 3.4-2: Density of several binaries, derived from lightcurves alone, as a function of the range in phase angle at which observations were made. The area shaded in grey shows the range of phase angles of MBAs. Note the large error bars in that area! (after Scheirich & Pravec, 2009)

With a angular resolution of 10 mas (at 133 nm, corresponding to 7 km at 1 AU of distance) and a sensitivity allowing the imaging of sources fainter than the visible magnitude 22, FDAI can spatially resolve many small binary asteroids in the main belt (see Fig 3). Asteroid masses will be derived from observations of the motion of asteroid satellites. By virtue of Kepler's third law, the orbital period and semi-major axis (determined from FDAI observations) of the binary asteroid uniquely determine the total system mass. FDAI can aim at asteroids with satellites discovered from photometric observations, revealing the presence of the satellite from eclipses. At least three visits per asteroids are required to determine the semi-major axis, the inclination and the eccentricity of the orbit (the orbital period is already known from the photometric observations at the discovery epoch). Given the orbital period and semimajoraxis, the mass of the system can be
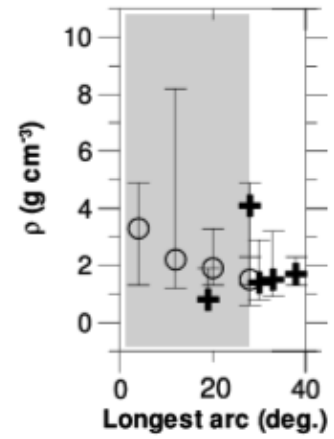

Figure 3.4-3 Binary asteroids in the Main Belt. The plot shows the separation of the two components vs the system magnitude at quadrature. The resolution domain of different instruments is shown

calculated. We note that WISE data provide sizes of the binary asteroids. Thus, the mass derived from FDAI and photometric measurements, divided by the volume of the components – the latter obtained from WISE sizes - will yield the bulk density of the system. Given an asteroid bulk density, we can proceed to derive insights into the asteroid's internal structure: namely the large-scale porosity, or macroporosity, by comparing the asteroid's bulk density with a typical meteorite analog bulk density. The first step in this process is to determine the asteroid mineralogy and match it with a mineralogy represented in the meteorite collection. This is done by comparing reflectance spectra of asteroids measured in the visible and/or near infrared wavelength range (0.4-2.5 μm) with laboratory measurements of meteorites. The comparison of the asteroid bulk density with the grain density of meteorite analogs yields the macroporosity of the asteroid.

Being given a total number of fields observable between 10000 and 13000 during the 5 years duration of the Fresnel imager mission, and assuming one third of these fields is dedicated to solar system science (4000 fields), an expected number of 398 asteroids will be found binary, and their size, shape and mass data precisely measured, leading to large increase of known densities on small solar system objects. The size measurements will provide a total of 1900 new values for asteroids.

In addition to main belt's asteroids, Kuiper belt's objects at 30 AU will be observable, with a resolution of 200 km. Small solar system bodies are not the only targets: The upper atmosphere auroras on Jupiter will be imaged at a resolution of 25 km in Lyman-α.

The tracking of faint asteroids will require steering the configuration and tracking the target. This will be done at no additional propellant cost, as long as their speed vector can be considered constant at the angular resolution and timescales considered (1000 to 10000 s). An unknown drift during the exposure is not an issue, as long as the acceleration is known and the target is kept close to the centre of the field: both the image and the speed vector can be recovered from photon counting data without prior knowledge on the position nor the speed (Morel, Koechlin, 1998).

4. Proposed mission profile to achieve these objectives

4.1 Preferred "Station-keeping Orbit" and "Transfer Trajectorie"

A large panorama of possible Earth orbits, Earth-Moon and Earth-Sun Lagrangian points have been studied.
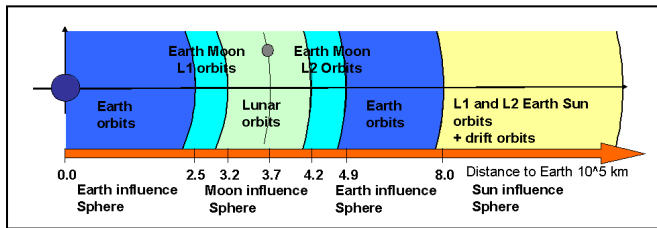
It has been proven that an Earth orbit cannot be competitive for astrophysical applications, even if very specific and optimized. Finally, only the L2 Lagrangian Earth-Sun domain has been selected because it is the only way to minimize the external disturbances as bodies' occultation, parasite light and gravity gradient force to be fought. At Earth-Sun L2, the only disturbing force remains the solar radiation pressure which is an important sizing case, as it will be shown later on.

The way to go is given by the 3-bodies gravitational equations. They show the family of possible trajectories. The figure on the right illustrates the equations results. Insertion into Large Lissajous orbits doesn't require any specific manoeuvre. The ΔV requirement is mainly for correcting the launcher trajectory uncertainties (ΔV ≈ 80m/s for a 6. 10^5 km radius one).

Inserting a spacecraft into a small Lissajous orbit requests additional ΔV (this is the case for Planck). For example, a 2.10^5km orbit requires 240 m/s of ΔV.

So, the preferred L2 orbit is a "Large Lissajous" type: radius between ≈ 6. 10^5 km and ≈ 8.10^5 km.
The ΔV need during the duration of the mission on this "Large Lissajous" is ≈ 40 m/s*. [Hinglais 2009]
Including consumption for safe mode and reaction wheels desaturation for each spacecraft for 5years. These estimations are performed taking into account the mass and moment of inertia of each spacecraft.
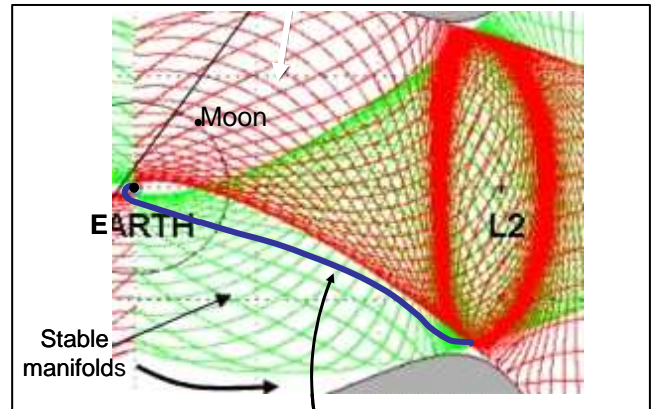
Natural and stable trajectory to reach a Lissajous orbit at L2

Velocity Increment need during the transfer trajectory between launcher injection and "Great Lissajous" type orbit: < 50 m/s (including consumption for safe mode and reaction wheels desaturation for each spacecraft*).

4.2 Preferred Launcher

In order to minimise launch mass for the two spacecrafts (Fresnel Array S/C + Receiver S/C), we propose a configuration where the Fresnel Array Spacecraft carries the Receiver Spacecraft in the launcher; In these conditions, the mass at launch is about 1750kg (See §6.4) whereas the use of carrier structure like "SPELTRA/Soyuz", for example, would lead to a mass above 2000kg (See §6.4).

Due to the smaller mass of the spacecrafts (~1750 kg total), the preferred launcher is a **Soyuz**. In fact, for a launch from Kourou and an injection to L2 "Large Lissajous or Hallo orbit", the performance of this launcher is 2100kg allowing a system mass margin of 350kg (> 21%) in "prephase A". In few years, the "New Soyuz" performance will be about 2300kg authorizing a system mass margin of 570kg (~33%).

4.3 Operational mode

This Fresnel Diffractive Array Imager (FDAI) mission in the UV can be shared in 3 main operational modes or phases: Launch phase, Transfer phase and Scientific Observation phase.

4.3.1 Launch &Transfer phase

The Receiver S/C and the Fresnel Array S/C will be injected by the launcher into a transfer trajectory from Low Earth Orbit to a "Large Lissajous" L2-orbit. Each spacecraft will travel separately during this transfer phase. In fact, the Fresnel Array membrane and sun-shield must be deployed as soon as possible after launch, to avoid mechanisms failure risks associated to long space conditions exposure. The tradeoffs, which includes satellites architecture, operations and mechanisms, show that it is better to operate the two satellites independently during their trip to L2, even if stacked at launch [cf. §4.2]. This waives studying and testing a third satellite (composed of both stacked in flight) and permits the commissioning in flight of each satellite separately.

4.3.2 Scientific Observation phase

This phase includes Formation Flying during the scientific observations (Orbit control, manoeuvre for scientific data acquisition, safe mode, ...). We briefly highlight some specific FDAI mission operations.

Beyond an almost classical trip, the L2 insertion and the formation flying problematic (discussed in § 6.1. GNC requirements and key issues), the FDAI particularities imply specific manoeuvres, which have to be optimised in the operation plan. They guarantee a high (targets number / mission lifetime) ratio and minimise the propellant budget, which is an important concern for FDAI missions:

- It's necessary to change the inter-satellite distance, when jumping from one wave band to another. There will be two or three such wave bands. This leads to grouping the targets, observe them all at given wave band, then to shift to another band and re-observe the same target group, rather than exploring all bands at each target. One can also group targets in a given region of the sky, thus requesting small line of sight changing manoeuvres, then steer the spacecraft configuration to another target group.

- Some high dynamic range observations require taking two images of the same field, differentiated by a rotation of at least ±10° around the line of sight to prevent risk of target masking by the PSF spikes [cf. § 5.3 Instrument Conceptual design]. This will double the observation time required per target and per band, but will not cost any propellant, as this spacecraft attitude rotation is done by reaction wheels.

- Last, the observable sky field turns with a one year period because the "Sun-Earth-L2" line rotates in the ecliptic plane. The visible sky field and the maximum duration of observation at a given point depend of the size of the sun shield [cf. fig. 4.5.-1]. For the UV, there is no need to shield from the earth or the moon. It may even be envisioned to operate without a sun baffle, which would allow a quasi-complete sky coverage at any time, but the effects of thermal dilatation of the main array have not been studied enough and we cannot guarantee it's possible for the moment, so we present here a solution with baffle protection for ±15° tilt angles.

4.4   Mission lifetime

The mission lifetime expected is 5 years. The quantity of onboard propellants had been sized for such lifetime.

4.5   Communication requirements

The great Lissajous orbit (radius < 8 10^5 km) imposes the geometry below for the communications [fig. 4.5-1]:
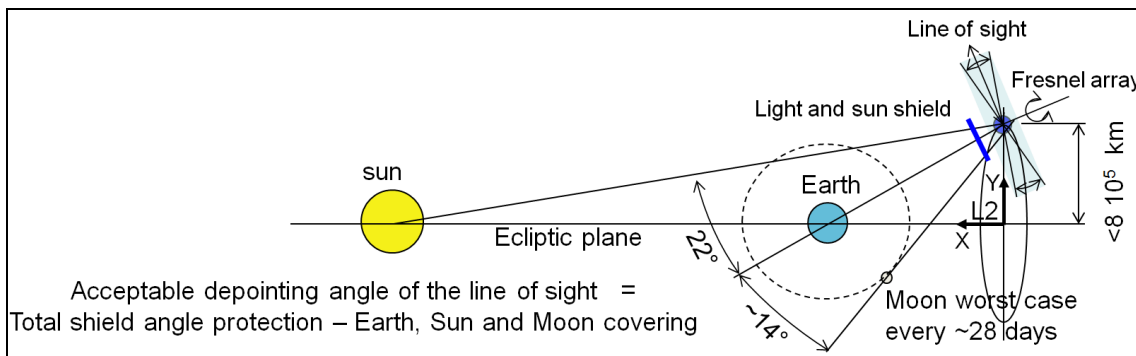

Fig 4.5-1: FDAI orbits

Hence a trade-off has to be found between the Lissajous size and the antenna performances. Fortunately it can be solved by using a Reflect-Array type antenna which allows configuring electronically the emission lobe in a cone of 140° with a 18 decibel gain. It is necessary to download the data during the scientific acquisitions because of the limited data transfer rate, the distance to Earth and the ground stations possibilities.

4.6   Ground segment assumptions

The ground segments needed would be the same as for other Lagrangian point operations. As for the Ground Station, this mission would use the 15 m antennas (band X). The download rate of data will be 0.78 Gigabyte per day. At L2 orbit, 8 hours a day visibility, are available for transfer: we arrived at 217 Kbit/s stream without compression. In the hypothesis of a compression rate of 1:3, the data rate is 72 Kbit/s.

5. Proposed model payload to achieve the science objectives

5.1. Overview of all proposed payload elements

The proposed two-satellite formation-flying FDAI (Fresnel Diffractive Array Imager) is as follows [fig. 5.1-1]:

- The first satellite holds the **Fresnel Array payload**.

It is made of the <u>spreadable Fresnel Array membrane</u>, its <u>unfolding structure</u> and <u>baffle</u>. This membrane constitutes the main optics of the Imager: it gathers incident light and focuses it into an intermediate image plane where the second spacecraft is located. The Fresnel Array is the entrance pupil of the instrument; so, its dimensions and geometry drive the angular resolution, the dynamic range and the sensitivity.

- The second satellite has the **Receiver Optics payload**.

It is located 15 to 20 kilometres downstream of the first satellite. It comprises a <u>field telescope</u>, and two wave band channels. Each channel comprises one <u>chromatism correction optic</u>, one <u>Very Accurate Navigation Sensor</u> (VANS) and one <u>scientific instrumentation set</u> (imager, spectro, detector). The mass budget has been calculated for three channels rather than two, in case some collaboration could pay for the additional cost of optics and detectors.

Let us define the determinant parameters of a FDAI payload:

Cgr	Square size of the Fresnel Array membrane optical aperture
N	"Fresnel Number": quantity of Fresnel zone coronas countable along the array half side
λc , $\Delta\lambda$	Central wavelength: $\lambda c = (\lambda max + \lambda min)/2$ and bandwidth of a science band: $\Delta\lambda = \lambda max - \lambda min$
Q	Wavefront quality level specification (expressed as $\Delta OPD < \lambda c / Q$, pick-valley)
F	Inter-spacecraft distance depending on spectral band: $F = Cgr^2 / (8\ N\ \lambda c\ )$ (eq.5.1-1)

The figure 5.1-1 shows the main parameters of the Formation Flying payload:

$\Delta\theta_L$: Angle between the FDAI Optical axis (Z_{OPT}) = [Oos OLP] and the target direction (Z_G)

Δx_L : Lateral shift between the centre of the Receiver Optics and the target line ($\Delta x_L \sim F \cdot \Delta\theta_L$)
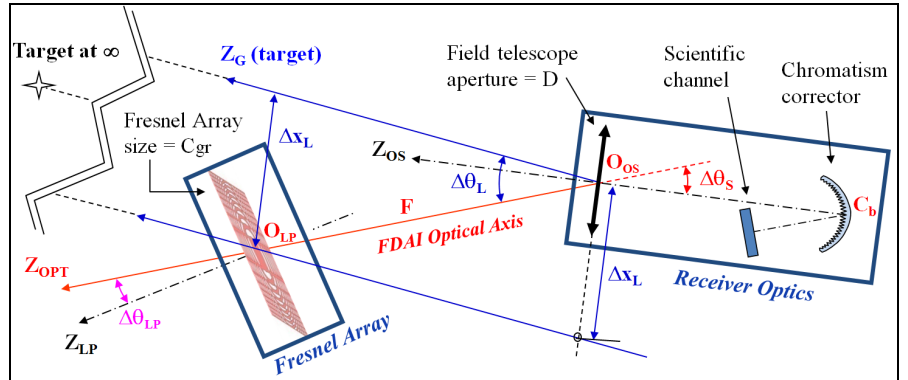

Fig 5.1-1: Overview of the whole FDAI-UV formation.

$\Delta\theta_S$: Angle between the FDAI Optical Axis (Z_{OPT}) and the Receiver Optics axis (Z_{OS}) = [Oos Cb].

$\Delta\theta_{LP}$: Angle between the main optical axis (Z_{OPT}) and the axis of the Fresnel Array (Z_{LP}).

We get a correct FDAI pointing with the three following actions:

1. Align (Z_{OPT}) with the target direction e.g. ($\Delta\theta_L \to 0$).
2. Align (Z_{OS}) with (Z_{OPT}) e.g. ($\Delta\theta_S \to 0$).
3. Align (Z_{LP}) with (Z_{OPT}) e.g. ($\Delta\theta_{LP} \to 0$).

Action 1 corresponds to the control of the relative lateral position Δx_L between both spacecrafts (translation).
Action 2 corresponds to the fine pointing of the Receiver Optics axis, towards the FDAI Optical Axis (attitude).
Action 3 corresponds to the pointing of the Fresnel Array Optical Axis, towards the FDAI Optical Axis (attitude).

5.2 Description of the measurement technique

We make an image, or a spectrum, or both, of the target. A UV photon-counting camera will provide the spatiotemporal coordinates of every incoming photon. Recording these (X, Y, t) triplets will allow reconstructing the images and spectra, which will be sent to ground. Raw photon coordinates may, if necessary, be downloaded, but only for a limited time of observation: because of the sparcity of photon data, reconstructed images and spectral data occupy much less data space.

5.3 Instrument conceptual design and key characteristics

The key payload is the Fresnel Array membrane: it brings diffraction limited imaging capability in the UV at an excellent rejection factor. It has the advantage of being lightweight, thin, deployable and relaxed in tolerances.
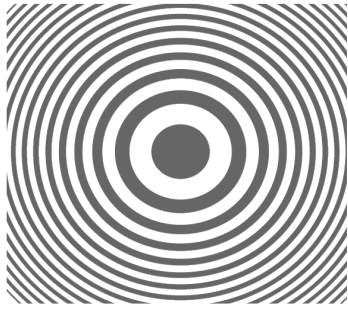

Fig 5.3-1: Original pattern of the Soret Zone Plate made of void concentric Fresnel zones coronas. Idealistic for optical need, but not feasible mechanically.
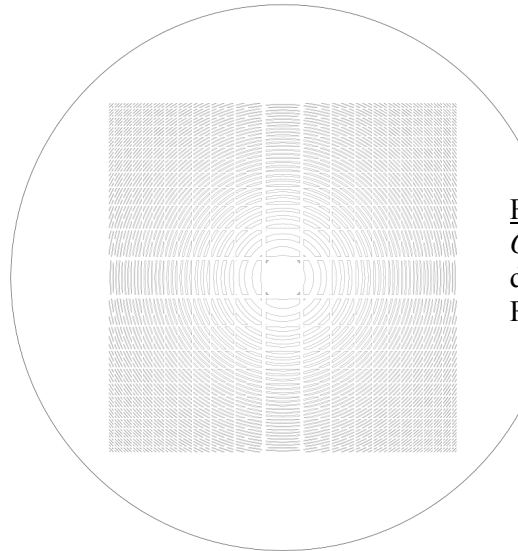

Fig 5.3-2: *Orthocircular* pattern designed for the Fresnel Array.

This opaque membrane is punched with hundred thousands of void subapertures, specifically shaped and positioned along Fresnel zones. An incoming wavefront, going across them, is focussed by diffraction, without resort to any reflective or refractive component.

As a binary grating, Fresnel Arrays focus only a fraction of the incident light in positive diffraction orders (+1 ; +3 ; +5 ...), the order 0 being a parallel beam.

For scientific imaging, we take advantage of the order +1, the most powerful of the diffraction orders (order -1 contains as much light, but diluted by its divergence). The angular resolution is that of a 4-m aperture. Order +1 images are not directly workable at wide spectral band, owing to axial chromatism intrinsic to diffraction optics: a complete chromatic correction is done in the Receiver Optics. The theoretical maximum throughput is $T_{+1} = 1/\pi^2 = 10.3$ % for regular concentric Fresnel coronas [fig. 5.3-1].

Notwithstanding, there is a trade-off between optical performances and mechanical constraints. We designed the *Orthocircular* pattern [fig. 5.3-2], that results from the intersection of Fresnel zone void coronas with orthogonal bars mesh, insuring mechanical cohesion of the whole structure. This orthogonal bars mesh, combined with a square optical aperture, preserves high rejection rate (high contrast) in the four quadrants of the field, except under the spikes [fig. 1.4-2]. Numerical simulations show that this geometry potentially features a relatively good transmission $T_{+1} \sim 6.8$ % and a high 1.10^{-8} rejection rate. To keep such a high dynamic range at closer than 10 resels from the central lobe of PSF, an apodization may be applied by subaperture size modulation. The 6.8 % transmission is obtained with a trade-off between apodisation and transmission.

The order 0 will feed the navigation channels, as it conveys $T_0 \sim 40$ % of incident light. It is blocked after the field optics and does not reach the science focal plane.

5.3.1 Genesis of a spreadable Fresnel Array membrane in space

	requisite	*Solution for space membrane.*
Membrane opacity at λ of interest to guarantee high rejection rate.	**T < 1.10⁻⁸**	Kapton foil coated with a 1 µm-thick layer of Aluminium that blocks UV from λ > 80 nm.
Positioning demands for subapertures to meet wavefront quality criterion (Q)	**Δr < Cgr / (4 N Q)** (eq.5.3-1)	Constant force springs keep the membrane in tension, admissible ΔT < 100 K. [fig. 5.3-3]

N.B : Only radial displacement (Δr) will have a significant impact on the OPD error .

Fig 5.3-3. Technical solutions to support and keep in tension the space membrane.

Constant force springs:
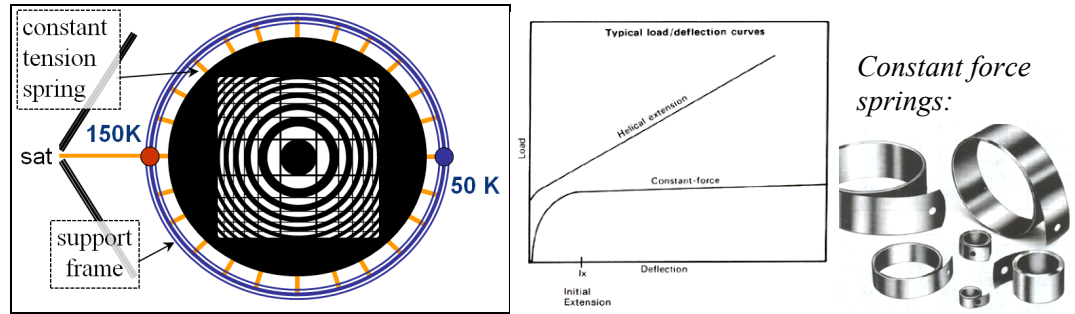
The useful optical aperture is square but the entire membrane is circular [fig. 5.3-3]. Revolution symmetry makes easier the deployment and the keeping in tension. In addition to orthogonal bars mesh, there would be hidden radials bars in the opaque parts: first to help the deployment, second to reinforce the membrane. Should its Thermal Expansion Coefficient (CTE) not be convenient, a heating device (250 Watts) might be used to cancel the temperature gradient.
The structure frame for deployment has been designed and validated [cf. fig 5.10-1]

5.3.2 General Receiver Optics architecture

The Receiver Optics is at the focal plane of the Fresnel Array [eq.5.1-1], which corresponds to the central wavelength of the selected science channel [fig. 5.3-4]. The two-mirror field telescope collects order +1 and order 0 beams, then reimages the Fresnel Array in a pupil plane where the achromatizers operate. The configuration off-centre avoids secondary mirror central obscuration of instantaneous field of view (IFOV) in science images.
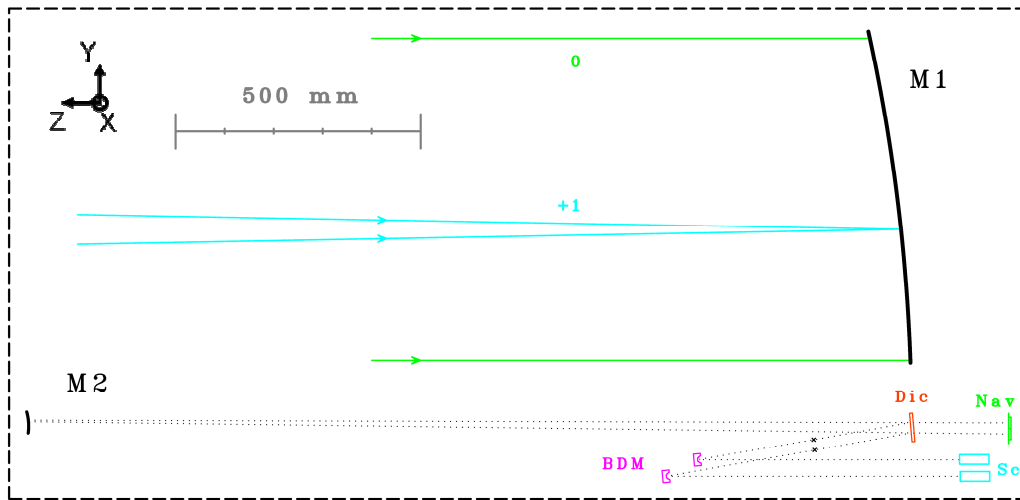

Fig 5.3-4: Receiver Optics scale drawing.

M1: primary mirror

M2: secondary mirror

Dic: dichroic beamsplitter.

BDM: blazed diffractive mirror (achromatizer)

Nav: navigation cameras

Sc: scientific instruments.

x: masks to block order 0

As *field* optics, M1 aperture diameter, **D**, fixes the maximum IFOV for science: $\theta_{½} \sim 4\,D\,N\,\lambda c\,/\,Cgr^2$ (eq.5.3-2)
On account of axial chromatism, beams away from λc are unfocussed and might be vignetted by M1 aperture: D also restrains the relative spectral band, $\Delta\lambda/\lambda c$, of a given science beam: $\Delta\lambda/\lambda c \sim D\,\sqrt{2}\,/\,Cgr$ (eq.5.3-3).

As seen from the scientific instruments, the field optics "telescope" lays in an intermediate image plane, contrarily to classical telescopes (such as HST or WSO-UV); therefore its optical surfacing is far less constraining, to preserve "high Q"-quality wavefront, and low scattering.

5.3.3 Optical architecture of scientific and navigation channels [fig. 5.3-4]

The phase 0 carried out at CNES concluded that science and navigation must share the same M1 aperture. Indeed, very accurate measurements of pointing and alignment angles defined in § 5.1 are mandatory for the GNC [cf. §. 5.6]. Coupled to scientific paths, the Very Accurate Navigation Sensors (VANS) uses the M1 mirror as entrance pupil, which provides them the angular resolution needed.
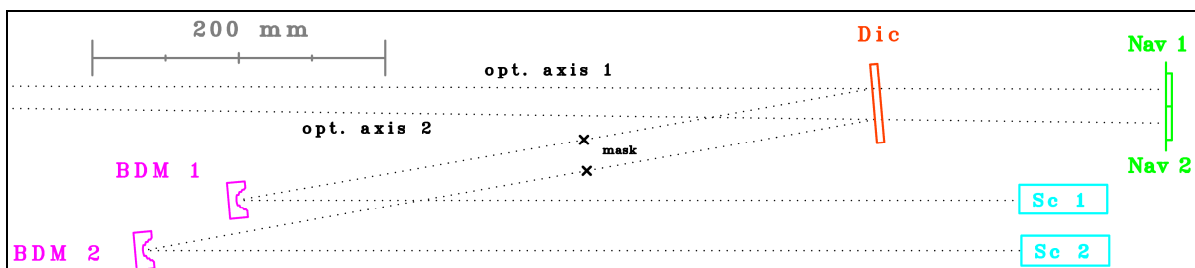

Fig. 5.3-5: scale drawing zoomed on optical architecture of science and navigation channels.

To separate scientific beams from navigation beams, a classical dichroic beamsplitter (Dic) is proposed. The spectral separation is as follow [fig. 5.3-5]: the dichroic beamsplitter reflects the two UV science bands and transmits NUV/VIS wavelengths for navigation.

There are two VANS cameras (Nav 1 & 2), one per science path. Complementary optics may be required near navigation sensors (to adapt their EFL for example). Figure 5.3-6 explains how $\Delta\theta_L$ and $\Delta\theta_s$ navigation angles are measured thanks to image of laser diodes in the membrane and image of guide stars.

VANS are supplied by order 0 beams but the latter are not desired for science: they are blocked downstream in the scientific paths by little masks (between BDM and Dic).

A sole channel is on at a time: how to switch from one science path to the other is detailed at § 5.7.2. end.
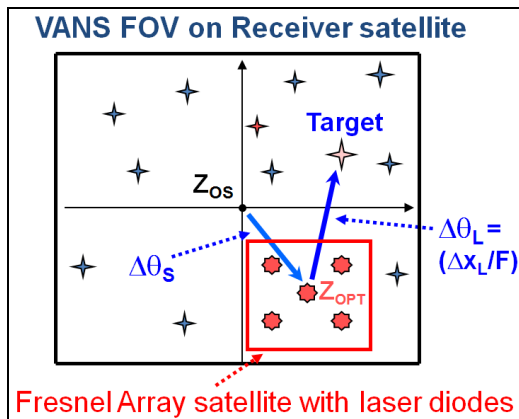

Fig 5.3-6: IFOV of VANS cameras and Fine Navigation

The navigation images, fed by order 0 beams, form at focal plane of field telescope.

Images of reference stars (or the target star) enable to compute $\Delta\theta_L$ **(2D)** and laser diodes image to measure $\Delta\theta_s$ **(2D).**

We propose an Active Pixel Sensor (APS) as 2D detector to acquire sources with important gap of brightness.

The GNC obliges an IFOV of VANS cameras wider than 3 times the Fresnel array angular size seen from the Receiver Spacecraft for making easier the Fresnel Array acquisition in the FOV of the VANS [See § 5.7.2 Coarse and fine ... acquisitions].

5.3.4 Chromatism correction strategy

Each science band has a specific chromatism corrector blazed at its λc. We went into a blazed diffractive mirror (BDM) that achieves both achromatization and focusing in a single reflection [fig. 5.3-5]. Its Fresnel zones, blazed at order –1, are engraved on a concave mirror that sheds the final image.

This correction scheme suits for broadband imaging in the UV using reflection only, glasses becoming opaque, and the fewest reflecting surfaces to minimize light scattering and throughput loss. It replaces blazed Fresnel lenses previously qualified in the VIS domain [Serre, 2009].

At this level, comes the choice of **Fs** , the effective focal length of field telescope. Let's remind the field telescope ought to reimage the Fresnel zones of the membrane and to superimpose them to those of BDM. The last zone on BDM must be large enough for feasibility reason: Fs is adjusted to grant sufficient lateral magnification.
Wmin being the smallest possible zone, we have: **Fs > Wmin Cgr / ($\lambda c \sqrt{2}$)**   (eq.5.3-4)
Considering Wmin = 3.4 µm, λc = 133 nm, Fs is set to 72 m. Such long focal length telescopes have already flown and can fit in 2-meter compactedness [fig. 5.3-4].

BDM pupils are very small ($\Phi b \sim 20$ mm) and have large curvature radius: Rc ~ 300 to 500 mm implying surface sags of 100-150 µm and F-numbers bigger than ~12. Optical simulations showed that a pure spherical profile may comply with wavefront grade need. Fresnel zones are likely to be engraved by photolithography and Reactive Ion etching (RIE) and polished by magnetorheology [cf. § 5.10].

Note: If a BDM is shifted, lateral chromatism appears: it behaves as a low resolution field spectrograph. This property can be exploited for gross spectro-imaging provided that extra Fresnel zones be added (to hinder vignetting when pupil shift). BDM translation can be done by the tip-tilt mechanism [fig. 5.9-1].

5.3.5 Coatings for optical surfaces in the Ultraviolet

Each surface will be applied a dedicated coatings to optimise its reflectivity. In the UV, Al/MgF2 layer stack are available yielding up to R > 85 %. Coating of M1 and M2 mirrors will reflect all science bands [120 - 190] nm, plus a VIS/NUV band to feed the VANS. Each BDM will have an optimized coating at its science waveband.

5.4 Performance assessment with respect to science objectives

The proposed FDAI has a primary aperture of **Cgr = 4** m, and a field telescope of **D = 0.68** m and a Fresnel number of **N = 750**. N is a very important parameter that impact on performances for science: the larger N is, the higher the contrast, the more IFOV we get, the more targets one can observe (indirectly because F are lesser). The two scientific channels offer these nominal performances:

	Waveband (nm)	λ_c (nm)	IFOV (½ field in arcsec); linear resels	Angular resolution (mas)
Science band n°1	117 – 148	133	**3,48** (1019 x 1019)	**6,8**
Science band n°2	150 – 190	170	**4,47** (1019 x 1019)	**8,8**

The image taken will be **1000 x 1000** element of resolution (resel) field.

5.4.1 Spectrograph
To resolve the spectral lines of Lyman-α continuum from 121 to 150 nm, the required resolution is $\lambda/\Delta\lambda$ =4000
These are performances which nowadays spectrographs can cope with. Ex: HIRDES and LSS spectrographs in WSO-UV.

5.4.2 Dynamic range and image quality attained
Scientific objectives → dynamic range → wavefront quality e.g. choice of Q criterion: Q = 6 to 8 is needed for classical imaging, Q > **25** for spectro-imaging of high contrasted sources. In fact, wavefront quality is mainly affected by the performances of optics payload in pupil plane: the membrane and the BDM.
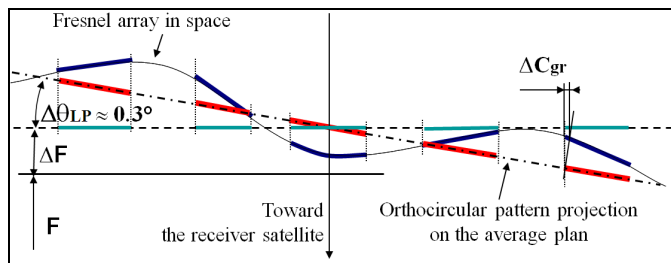

Fig 5.4-1: membrane performance needs vs. Q

What is significant on the wavefront quality is the radial displacement of the subaperture projection over the membrane average plane e.g. a radial error Δr.

Setting Q to 25, the tolerance is $\Delta r < 50$ μm [eq.5.3-1] and $\Delta\theta_{LP} < 0.3°$ for array warping.

The membrane performances are expressed in [fig. 5.4-1]. Owing to its comfortable uncertainties, membranes of this kind should output very pure UV wavefront. Note that mirrors are disadvantaged in the UV: the tolerance on their surface defects is $\Delta z < \lambda / (2\,Q)$ which is relatively stringent.
We are confident about BDMs which feature little size, geometrical specifications not such tough: surgical micro-optics surfacing permits to control the surface irregularities better than $\Delta z < 5$ nm. [cf. § 5.10].

That's why FDAI-UV features diffraction limited image: 0.007" resolution, 10^{-4} rejection rates expected, and 1.10^{-6} rejection rates expected at 10 resels from central lobe. These values are from extrapolation of the visible band tests and numerical simulations. Optical tests in UV are scheduled for early 2011.

5.4.3 Photometric performances

The following throughputs are assumed: T_{+1} ~6.8 %, M1 and M2: 85 %, Dic: 90 %, BDM: 85 %.
- Global throughput: **3.76 %**
- Equivalent collecting area: **6014** cm².
- Assuming exposure time of 3600 s and SNR > 3, the sensitivity rises to **Mb ~= 23**.

5.4.5 Reachable quantity of targets and observable sky

It is the same strategy as HERSCHEL and INTEGRAL (ESA). It covers a meridian band of +/- 15 degrees [cf. fig. 4.5-1] whose axis is towards the Sun: 10000 to 13000 fields observable (for example 3000 fields would yield 600 binary asteroids masses and densities).

5.5 Resources: mass, volume, power, on board data handling and telemetry

On-board memory for one week storage (in case of ground station unavailability), taking into account § 4.6.: at least **8 Gbyte** in the Receiver spacecraft. **1 Gbyte** will be enough in the F.A. spacecraft for servitudes.

The Fresnel Array payload mass budget is **66** kg:

	Unfolding & I/S	Structure	Membrane	Springs	Sun shield	TOTAL
Weight (kg)	4	11	5	10	31	**66**

Table 5.5-1. Mass budget of spreadable Fresnel Array membrane, structure and baffle in kg.

A scientific channel is estimated at 40 kg. For a 2 channel scenario, the payload mass budget is **196** kg:

	Two science channels	Baffling (20 % of 80 kg)	field telescope	TOTAL
Weight (kg)	80	16	100	**196**

Table 5.5-2. Mass budget of Receiver payload in kg

N.B: At phase 0, it was estimated that adding an optional third channel increases the mass to 263 kg.

Power budgets are detailed in § 6.4.

Communications by Radio Frequency is necessary for inter-satellite communications:

* R. Payload sends to F.A. Payload: VANS measurements & estimations, RFS inter-spacecraft distances, commands for laser diodes.

* F.A. Payload sends to R. Payload: attitude coordinates of F.A. S/C, RFS inter-spacecraft distances (redundant).

5.6 Pointing and alignment requirements

The main parameters to be controlled by the Formation Flying Guidance Navigation & Control are [fig .5.1-1]:

- The FDAI inter-spacecraft distance (***great focal***): $F(\lambda c) = Cgr^2 / (8 N \lambda c)$
- The FDAI optical axis pointing uncertainty $\Delta\theta_L$ and its initial value $\Delta\theta_{Li}$ while fine acquisition for target tracking by the Receiver field optics aperture.
- The lateral positioning tolerance between the Receiver Satellite w.r.t. the Fresnel Array satellite: Δx_L
- The Receiver optical axis pointing uncertainties w.r.t. the FDAI optical axis: $\Delta\theta_S$
- The Fresnel Array optical axis attitude, $\Delta\theta_{LP}$

From these definitions, it was established the following relations that express the fine pointing requirements:

FDAI pointing tolerance	Lateral position tolerance	Great focal tolerance	Receiver attitude tolerance	Fresnel Array attitude tolerance *
$\Delta\theta_L < \lambda c / Cgr$	$\Delta x_L < Cgr / (8N)$	$\Delta F < F/(4NQ)$	$\Delta\theta_S < \lambda c^2 / (Cgr \, \Delta\lambda)$	$\Delta\theta_{LP} < 0.3°$

Table 5.6-1: Main parameter tolerances (Fresnel Arrays make it very released the requirement on $\Delta\theta_{LP}$)*

- Navigation will be done by **angular** measurements from the VANS but the command and actuators will proceed to relative lateral **translations** between the two satellites (Δx_L in 2D).
- Receiver optics pointing error ($\Delta\theta_S$) impacts on the residual chromatism in the image.
- Initial alignment ($\Delta\theta_{Li}$) consists of target acquisition in the Receiver optics IFOV: $\Delta\theta_{Li} < 5.6 N \Delta\lambda / Cgr$

The great focal tolerances are not stringent, nevertheless, they will be taken smaller in the following to limit the "longitudinal position (F) / Attitude ($\Delta\theta_S \rightarrow \Delta\theta_L$)/ lateral position ($\Delta x_L$)" coupling $\Delta x_L = F \Delta\theta_L$

Below are the main parameters values and the corresponding requirements:

λc (nm)	$\Delta\lambda$ (nm)	Cgr (m)	Q	N	F (km)	ΔF (m)	$\Delta\theta_{Li}$ (µrd)	$\Delta\theta_L$ (nrd)	Δx_L (mm)	$\Delta\theta_S$ (nrd)
133	31	4	25	750	20.1	± 0.30	± 33	± 33	± 0.7	±142
170	40				15.7	± 0.21	± 42	± 43	± 0.7	± 181

Table 5.6-2: 4-m FDAI numerical values of requirements (nrd: nanoradian)

Note 1: The four parameters $\Delta\theta_L$, $\Delta\theta_{Li}$, Δx_L and $\Delta\theta_S$ are two-dimensional and the corresponding value (under the parameter) is the requirement according to both of them.

Note 2: $\Delta\theta_L$ angles are the tightest, thus drive the resolution of VANS. The M1 mirror aperture confers them a diffraction limit at λ / D. To reach the demand on $\Delta\theta_L$, VANS work in "barycentric mode processing", which allows an angular accuracy of about 1/20 of (λ / D).

5.7 Operating modes

The FDAI Formation Flying has 4 main operating modes:

5.7.1 Astrophysical target change and/or great focal (F) modification

- In the great focal modification mode, we adjust F to select the scientific waveband at which the target is observed. Inter-spacecraft distances are tens of kilometers [Table 5.6-2], consequently a great focal length modification represents a several kilometers travel.

Example: A travel from F = 15.7 km to F = 20.1 km in ~2.5 hours consumes ~0.46 kg of hydrazine, in the hypothesis of ±0.5 m/s velocity increment.

- In the astrophysical target change, we point another target. The Fresnel Imager "pointing" is determined by the orientation of the FDAI optical axis linking both spacecrafts, and by the orientation of the receiver optical axis.

So, pointing is modified by a translation of one spacecraft with respect to the other (in a direction perpendicular to focal change) and an attitude correction for both spacecraft. A repointing is a process similar to a great focal change. For instance, a repointing of 5.7° when spacecraft are distant of 20.1 km corresponds to a 2 km travel. Great Focal change and repointing maneuvers can be combined to minimize the fuel consumption.

5.7.2 Coarse and fine "pointing and alignment" acquisitions

The best level of fine "pointing and alignment" accuracies for the FDAI Formation Flying is very restricting with Δx_L = ±0.7mm in lateral position corresponding to ±33nrd (resp. ±43nrd) for the main optical axis orientation and ±142nrd (resp. ±181nrd) for the receiver axis pointing of the "Channel 133nm" (resp. "Channel 170nm"). On account of this very fine "pointing and alignment" accuracy, 2 acquisition levels are inescapable [cf. §5.6]:

- **A first acquisition level is to acquire the Fresnel Array in the VANS IFOV.**

A Standard Stellar Sensor (SSS) (Accuracy ~10arcsec for ~ (10°)² IFOV), Gyros and Radio Frequency Sensor (RFS), on the Receiver Spacecraft, allow to acquire the Laser diodes of the Fresnel Array in the SSS IFOV. The RFS measurement allows determining the coarse direction (accuracy ~1°) of the Fresnel Array in the SSS IFOV of the Receiver Spacecraft. Simultaneously, the attitude control of the Fresnel Array Spacecraft (using its Standard Stellar Sensor and gyros for attitude measurement) has to ensure that its coarse attitude is close to that of the Receiver Spacecraft. For this preliminary acquisition, the VANS IFOV have to reach, at least, 3 times the FOV of the Fresnel Array seen from the Receiver Payload [cf. fig. 5.3-6 & Table 5.6-2], e.g. > 3 Cgr/F (> 597 µrd for the "Channel 133 nm" and > 764 µrd for the "Channel 170 nm").

This acquisition is realized by the same attitude change of both spacecrafts: they only use reaction wheels as actuators for attitude change & control, without the need of specific desaturations.

- **A second acquisition level with the VANS "Channel 133nm" (or the VANS "Channel 170nm").**

The main objective of this acquisition is to direct the FDAI axis toward the scientific target (generally a "Stellar Pattern"). This acquisition have to be divided in 2 phases: The 1st phase is to align coarsely the Receiver Payload and the Fresnel Array with the "Target Pattern". The 2nd phase achieves the fine "pointing and alignment" of the Receiver Payload, the Fresnel Array and the scientific target.

. The 1st phase must be performed with "SSS + Gyros + RFS" as attitude & position sensors and reaction wheels as attitude actuators on both spacecrafts. An Hydrazine Propulsion System on the Fresnel Array S/C allows to align coarsely the Receiver and the Fresnel Array toward the "Target Pattern" in the same way as "Astrophysical target change mode" (see § 5.7.1). This maneuver is performed by RendezVous (RdV) between the Fresnel Array S/C and a "virtual space point" located at a distance F (great focal length) from the Receiver S/C in the target direction. If we consider the example at the end of § 5.7.1, with a Fresnel Array S/C travel of 2 km, the coarse manoeuvre duration is about 4250s for 0.46 kg of Hydrazine consumption. During both velocity increments Fresnel Array S/C attitude has to be such that Hydrazine thrusters are properly oriented. Between the velocity increments (of 4000s on the last example), for safety reason, the Receiver S/C attitude has to be such that the laser diodes on the Fresnel Array are in the VANS IFOV. For that reason, a closed loop between the "VANS + SSS + Gyros" and the reaction wheels on the Receiver S/C is essential and, simultaneously, the "RFS + SSS" (on the Receiver S/C) allow to check the good development of the "Fresnel Array travel".

. The 2nd phase is to align precisely the Receiver Payload and the Fresnel Array with the "Target Pattern".

At the end of the 1st phase the Fresnel Array are in the VANS IFOV and the "Target Pattern" in the SSS IFOV of the Receiver S/C but, probably not in the VANS IFOV. Indeed, a rough estimate of the 1st phase RdV accuracy is ~1° (~ 400m) for alignment and F/50 (~ 400m) for the inter-satellite distance. During this 2nd phase, the main measurements are performed by the RFS (distance) and the SSS ("Target Pattern" direction), both sensors being on the Receiver S/C. Since concerning the 1st phase, hydrazine thrusters are used as actuators and the strategy is iterative. In general, one iteration is sufficient to get the RdV with the "virtual space point". In fact, if we consider the worst case (400 m error in all direction), the final error will be less than 8 m in all directions [cf. fig. 5.3-6].

Since the VANS IFOV is greater than 12m [fig. 5.3-6] this 2nd phase of the acquisition is successfully.
Note: before a scientific acquisition, the adequate science path has to be selected. To do so, the beams are deviated by a slight attitude change (< 0.1°) of the whole Receiver S/C.

5.7.3 On-board storage and image data processing
The data stored on-board are the photon coordinates data, transformed into images and spectral data.

5.7.4 Scientific data acquisition
During a scientific image accumulation, a servo control loop continuously maintains Δx_L, $\Delta\theta_L$ and $\Delta\theta_S$ within the requirements.
- In pure imaging mode: luminosity maps of 4000x4000 pixels are recorded and stored. This phase may last a few thousand seconds.
- In spectro-imaging mode: 20x20 fields are scrutinized, in each resel the spectrum is recorded.
- In photon-counting mode, data are continuously accumulated and processed. It consists of recording (X,Y, t) triplets of every incoming photons.

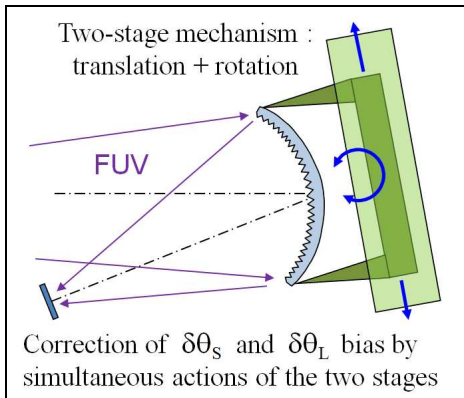## 5.8 Specific interface requirements: configuration needs, thermal needs

- Cryogenic temperature for the membrane (in the range of 50 – 150 K).

- In the UV no cooling device is necessary at focal plane.

5.9 Calibration and other specific requirements

Thermo-elastic deformations in the Receiver satellite may generate permanent misalignment of:
- The chromatism corrector, which results in a **$\delta\theta_{S(cal)}$** bias.
- The image plane, which corresponds to a **$\delta\theta_{L(cal)}$** bias.

We get rid of these biases thanks to tip-tilt and piezo actuators as explained in fig 5.9-1.

Two-stage mechanism : translation + rotation

FUV

Correction of $\delta\theta_S$ and $\delta\theta_L$ bias by simultaneous actions of the two stages

Fig 5.9-1: The chromatism corrector is mounted on a two-stage mechanism having four degrees of freedom: (ΔX ΔY) translations are done by the piezo stage, ($\Delta\theta X$ $\Delta\theta Y$) rotations by the tip-tilt stage.

Biases will be identified periodically by the analysis of scientific images. We suppress them like that:

$\Delta\theta X$ and $\Delta\theta Y$ actuations will reposition the image spot at the entrance of the focal instrument and thereby compensate for $\delta\theta L(cal)$ bias.

ΔX and ΔY translations will realign the chromatism corrector and thereby cancel the $\delta\theta S(cal)$ bias.

As in many optical space observatories, a standard re-focussing device would be needed.

5.10 Current heritage and Technology Readiness Level (TRL)

Payload unit	Actual developments	TRL	Improvements to be scheduled
Spreadable membrane	Current R&T on membrane telescopes	03	Manufacture and qualification of full scale Fresnel Array membranes (1 m < size < 4 m)
Fresnel Array	200 mm square, 696 Fresnel zone Arrays were carved and tested optically on sky sources.	04	Pattern geometry improvement (efficiency T+1, apodization...)
Unfolding Structure	A full scale prototype was made and qualified by *BTS industrie*.	04 [1]	Validate the unfolding structure for space environment
UV Mirrors (field telescope...)	Such mirrors should be ready to operate in space.	06	Off-axis mirror prototype that covers the UV region (from 110 nm)
Chromatism corrector by diffractive mirrors for the UV	Feasibility R&T in process. An UV breadboard will soon validate the blazed diffractive mirror.	03 [2]	Manufacturing process of the "blazed diffractive Fresnel mirror". Optimize the polishing process for grating grooves and roughness removing. Apply UV coatings and assess its performances.
Chromatism corrector by refraction	Corroborated by blazed Fresnel lens prototypes in VIS/NIR bands. (696-zone 58-mm, custom designed and built).	04	
Two-stage mechanism with 4 d.o.f.	Piezo-stages have flown separately	07	
VANS	Principle is near stellar sensor	03	Build a VANS integrated in the instrument.
Whole FDAI instrument	Qualified in the VIS, both on artificial targets and on real astrophysical sources by two FDAI breadboards. They are diffraction limited, have broadband imaging capability with 6.10^{-6} proven dynamic range.	04	Validate a model of FDAI in a relevant environment, in the UV domain.

**(1)** Validation of deployment structure by *BTS industrie* (assessment on metrology bench)*:*

* can be fold and unfold: preeminent for AIT at ground; constant-velocity deployment is warranted.

* Its segment bars are in Aluminium and entail excellent conductivity of heat.

* Obtained out of plane deformation: 0.6 mm in the worst case. It is under the tolerance ($\Delta z < 5$ mm) that guarantees array warping $\Delta\theta_{LP} < 0.1°$.

* The excursion budget for constant force springs is $\Delta L_{max} < 7$ mm. This specification is fulfilled with an obtained stretching of $\Delta L < 2.5$ mm (worst case).

* Fundamental vibration modes are above 7.8 Hz. $\rightarrow$ behaves as a rigid body from the GNC in fine pointing and alignment mode except when operating hydrazine propulsion.

Fig 5.10-1: photographs of structure prototype (mass: 10.3 kg) folding and unfolding.

(2) In the UV, roughness is a real concern for mirrors. With the consent of *RTRA-STAE* funding, the feasibility of BDM is in progress:

   * *SILIOS technologie* has demonstrated the ability to carve Fresnel zones in a concave substrate.
   * At *SESO*, trials with a new polishing machine by magnetorheology render exquisite preciseness [fig. 5.10-2]
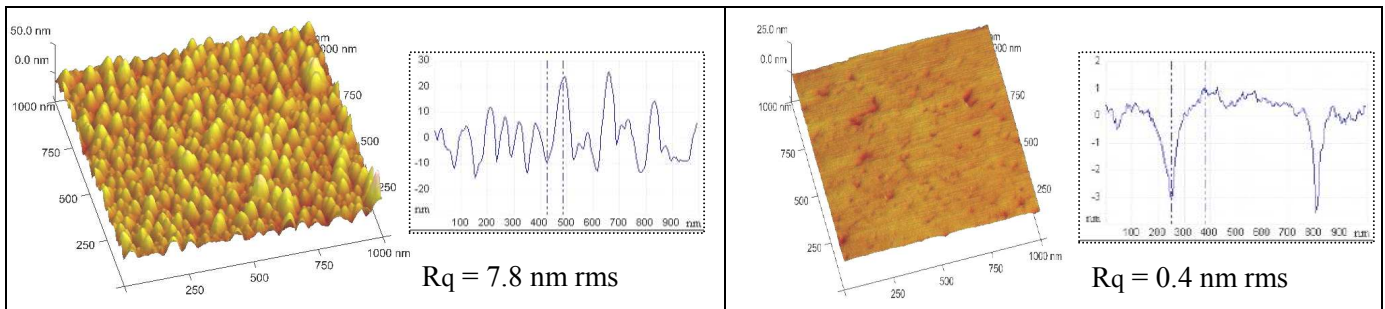
Fig 5.10-2: topographies of a 1µm x 1µm region in a same Fresnel zone scanned by an atomic force microscope (AFM), courtesy of "quality assurance service AQ/LE" at CNES. *On the left:* ion etching has induced a quadratic roughness of Rq = 7.8 nm rms. *On the right:* polishing by magnetorheology has really reduced the roughness (Rq < 0.4 nm rms).

This polishing technology will likely prepare surfaces to reflect prime quality UV wavefront: the small optics in the Receiver payload (M2, Dic, BDM) may be applied magnetorheology runs.

5.11   Proposed procurement approach

The equipment proposed is mostly "off the shelf": receiver UV optics, detectors. They are all developed in Europe (ITAR-free).

5.12   Critical issues

The membrane is a technology under development by an ESA contract to Centre Spatial de Liège, and we will also contribute to the development of Fresnel Arrays.

The chromatic correction grating is being assessed at SESO and SILIOS, under a RTRA-STAE contract. The optics are not tested yet (optical tests results expected mid 2011) but the results obtained on surface quality are promising.

See also § 8.1.

6. System requirements and Formation Flying key issues

6.1 Guidance Navigation and Control (GNC)

6.1.1. Fine "pointing and alignment" of this Formation Flying GNC (FFGNC)

The figure 6.1-1 hereafter and § 5.6 presents the main parameters that have to be controlled by the GNC during the scientific observations (Fine "pointing and alignment" mode). Two parameters are especially constraining:
- The lateral positioning uncertainty between the Receiver Satellite w.r.t. the Fresnel Array satellite: Δx_L (2D)
- The Receiver optics pointing uncertainty: $\Delta \theta_S$ (2D)

Fig 6.1-1 Simplified sketch of the Formation Flying configuration and geometry.
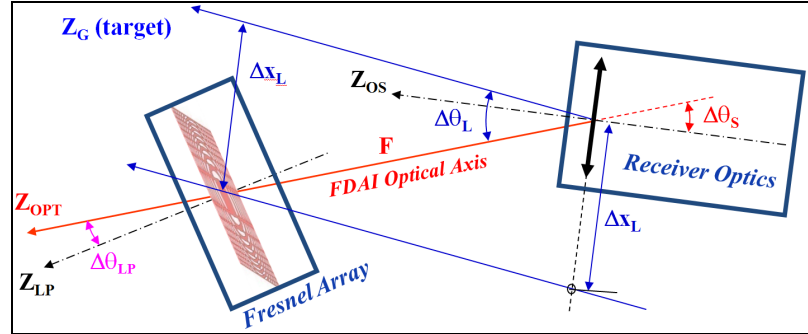
Indeed, the requirement on the uncertainty of Δx_L is better than ±0.7mm and the measurement of this parameter is angular by the VANS: $\Delta \theta_L = \Delta x_L / F$ (cf § 5.3-3 and fig.5.3-5). This Δx_L requirement represents an angular value of ±33nm for the VANS "Channel 133nm" and ±43nm for the VANS "Channel 170nm". Likewise, the Receiver optics pointing uncertainty $\Delta \theta_S$ is specified ±142nrd (or ± 181nrd) for the Channel "133nm" (or "170nm").

6.1.2. Very Fine GNC of the Fresnel array Spacecraft

Moreover, the requirement of the Fresnel Array S/C pointing uncertainty ($\Delta \theta_{LP} < 0,1°$) are less restricting than the one of the Receiver S/C ($\Delta \theta_S < 140nrd$ or 180nrd Channel "133nm" or "170nm"). This situation led to separate the position control (Δx_L) from the attitude control ($\Delta \theta_S$) of the Receiver S/C and, accordingly, to carry out the 3D position control (Δx_L and F) on the Fresnel Array S/C. Then we showed in [Hinglais 2009] that the fine relative position control of the Fresnel Array S/C is able to use cold gas propulsion system as fine actuators.
This cold gas propulsion system is working in "Pulse Width Modulation" and thresholding. For instance, if we choose a threshold on Δx_L, Sx = 0.1mm with a solar flux force of 60µN we calculate a medium periodicity of cold gas pulses T#146s [cf. fig. 6.1-2 opposite], that is to say a maximum of one million impulses by thruster for a 5 years mission lifetime. We consider that cold gas thrusters have a thrust of 10mN for a Fresnel Array Satellite instantaneous mass of 800kg [cf. fig .6.1-3]. With this hypothesis, the consumption of cold gas is 50kg (5yrs with 30% margin). The total number of cold gas thrusters is 26 (13 nominal & 13redundant). During this relative position control, 4 reaction wheels, 4 FOG & 2 SSS (nominal + redundant) assure attitude
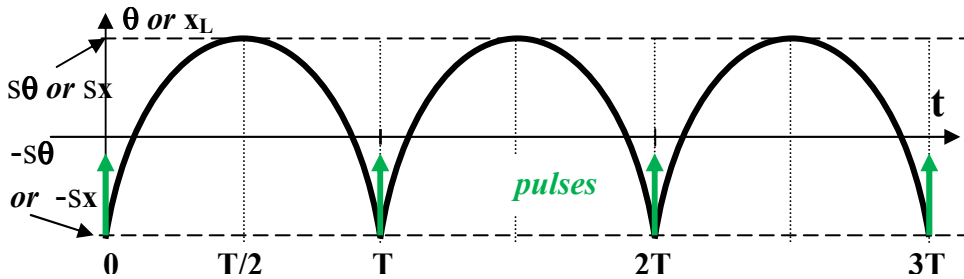
Fig. 6.1-2 : Propulsion mode by Pulse Width Modulation (PWM) and thresholding.

Cold gas propulsion system   F = 10 mN for Fine Relative Position Control (fixed thrusters on the Fresnel Array Platform)

Solar flux resultant force ≈ 60 µN for a 4 m membrane

Naturally stable system

Fig 6.1-3: Fresnel Array Spacecraft Fine GNC Principle
control of the Fresnel Array S/C with an accuracy of 0.05° (stability of 0.05° / 10h). Wheels desaturation will be

operated continuously with the cold gas propulsion system during this very fine attitude control and hydrazine propulsion system will be only used when we do not observe (daily, weekly,.....).

6.1.3. Very Fine GNC of the Receiver S/C

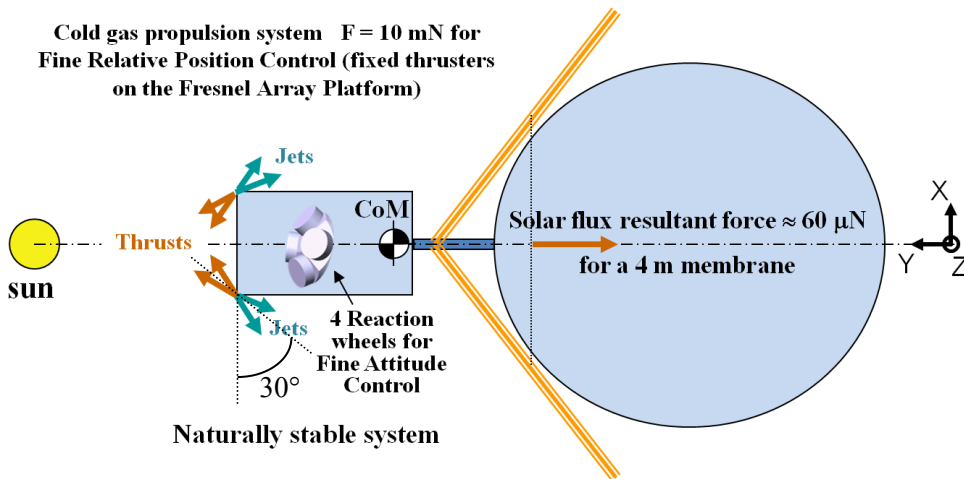The fine GNC mainly has to assure attitude control of the Receiver S/C with an accuracy of 140nrd or 180nrd Channel "133nm" or "170nm". This very fine attitude is measured by the VANS with an accuracy of about 40nrd. So, reaction wheels of the Receiver S/C have to activate its attitude with a stability better than ~100nrd (~20mas). The reaction wheels desaturation will be realize by Hydrazine propulsion system only used when we do not observe science sources (in synchronisation with the Fresnel Array S/C desaturation).

6.1.4. Modes of the Formation Flying GNC:

- **Transfer phase mode**:

Both satellites fly separately and perform their attitude and orbit control ($\rightarrow$ SSS + Gyro | reaction wheels + hydrazine). The first tests in flight of RF sensor FF-loop should be carried out.

- **Scientific observation phase modes**:

- First coarse acquisition: *On R. S/C* $\rightarrow$ RFS + SSS + Gyro + VANS | reaction wheels.
On F.A. S/C $\rightarrow$ RFS (redundancy) + SSS + Gyro | reaction wheels. [§ 5.7.2] .

- Second coarse acquisition: *On R. S/C* $\rightarrow$ RFS + SSS + Gyro + VANS | reaction wheels.
On F.A. S/C $\rightarrow$ RFS (redundancy) + SSS + Gyro | reaction wheels + hydrazine. [§ 5.7.2]

- Target change / inter-satellite dist. change: *On R. S/C* $\rightarrow$ RFS + SSS + Gyro | reaction wheels.
On F.A. S/C $\rightarrow$ RFS (redundancy) + SSS + Gyro | reaction wheels + hydrazine. [§ 5.7.1]

- Very fine acquisition: *On R. S/C* $\rightarrow$ RFS + SSS + Gyro + VANS | reaction wheels.
On F.A. S/C $\rightarrow$ RFS (redundancy) + SSS + Gyro | reaction wheels + cold gas propulsion system. The purpose is to switch form coarse to fine acquisition: in the *VANS image*, the target pattern enters inside the F.A. image. [tab. 5.6-2]. At the end, we get $\Delta\theta_L < \Delta\theta_{Li}$ such as $\Delta\theta_{Li} < 33$ µrd (or 42 µrd for "channel 170nm").

- Very fine pointing and alignment mode: detailed in § 6.1.
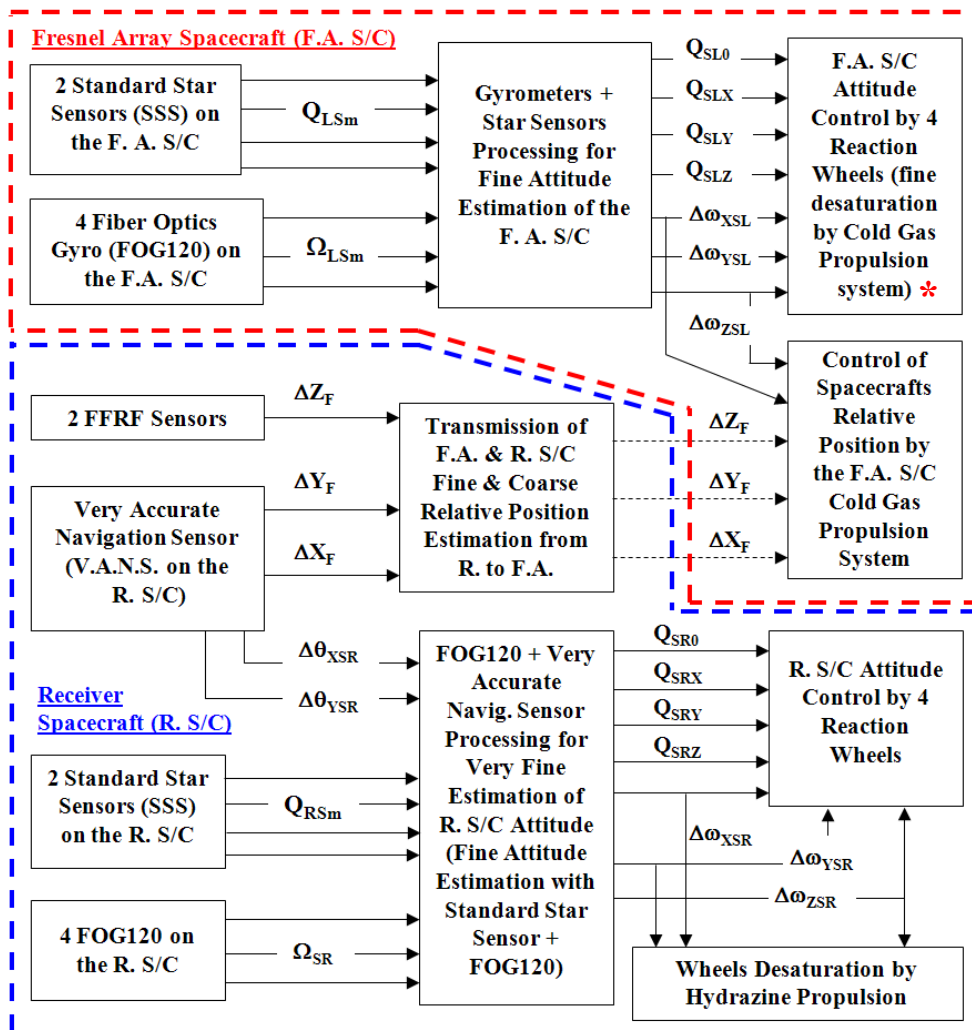

Fig 6.1-4 Formation Flying GNC functional architecture (*Hydrazine for desaturation § 6.1.3*).

6.2 On-board data handling and telemetry

LGA are operated in transfer phase on both satellites for telemetry and telecommands.

An MGA, located in the the R. S/C, will operate in observation phase to send scientific data. As a MGA, a Reflect-Array [fig. 6.2-1] is compulsory: otherwise, a 2-axis rotation antenna would jeopardize the R. S/C very fine attitude (because of dynamics disturbances)

In parallel, thanks to an Inter Satellite Link (ISL), F. A. S/C data will be transferred to the R. S/C. Then overall data are sent to Earth via the Reflect-Array antenna.
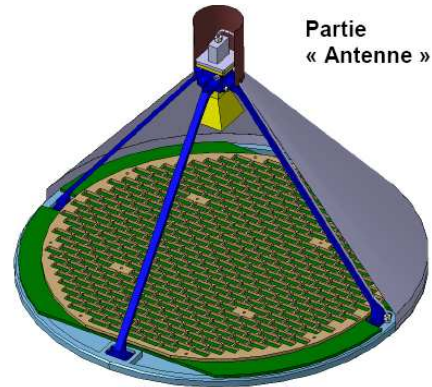
Fig 6.2-1: Reflect-Array antenna in the R. S/C

6.3 Mission operations concept (ground segment)

* To retrieve scientific data: one ground based, 15m antenna, 8 hours a day during business hours.

* Operating modes, (send targets coordinates, commands...) defined by the ground segment consortium.

* Occasionally proceeds to L2 Lissajous orbit corrections, once every 2 to 4 weeks. The telemetry data has been taken into account for the data rate.

6.4 Estimated overall resources (mass and power)

Unfolded R. S/C

Unfolded F. A. S/C

Stacked satellites at launch in the Soyouz fairing.

- R. S/C

- F.A. S/C

Folded F. A. S/C
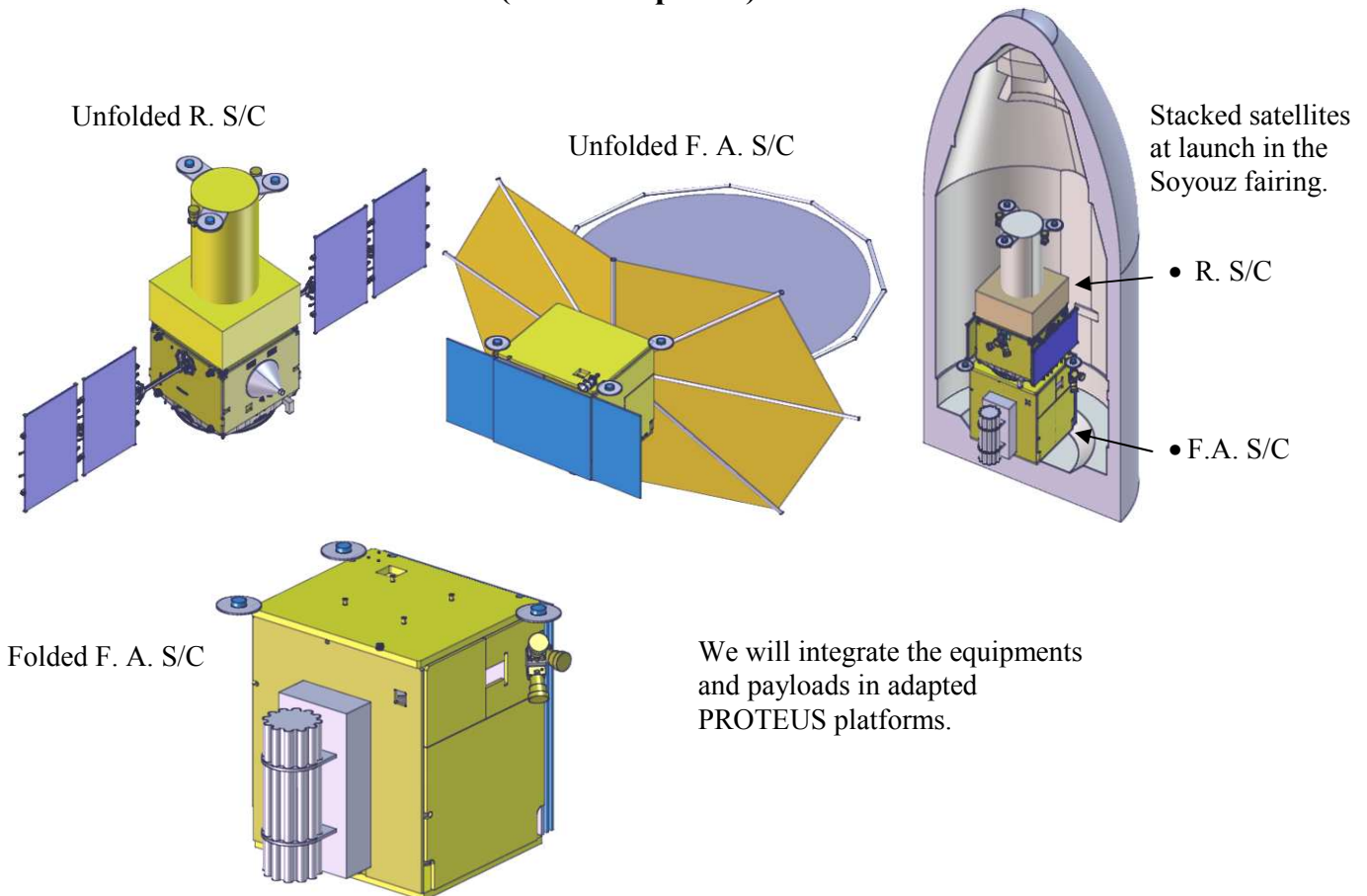
We will integrate the equipments and payloads in adapted PROTEUS platforms.

Mass, Power consumption and ΔV budgets were assessed by *Thales Alenia Space*:

	Receiver Satellite			Fresnel Array Satellite		
	Nominal	Margin	Max	Nominal	Margin	Max
Payload	180 kg	20%	216 kg	63 kg	20%	76 kg
AOCS	38 kg	5%	40 kg	38 kg	5%	40 kg
FF Units	26 kg	20%	31 kg	21 kg	20%	25 kg
OBC & Communications	36 kg	15%	41 kg	31 kg	15%	36 kg
Hydrazine Propulsion	8 kg	5%	8 kg	21 kg	5%	23 kg
Cold Gas Propulsion				56 kg	5%	59 kg
Harness	22 kg	20%	26 kg	26 kg	20%	65 kg
Thermal Control	13 kg	20%	16 kg	23 kg	20%	30 kg
Power	54 kg	5%	57 kg	58 kg	5%	61 kg
Structure	57 kg	10%	63 kg	178 kg	10%	196 kg
Total Dry	434 kg	15%	498 kg	515 kg	19%	610 kg
System margin		20%	100 kg		20%	122 kg
Maximum Dry Mass	Total Dry with margin		598 kg			733 kg

	Receiver Sat.	F.A. Sat.
Payload Dry Mass	216 kg	76 kg
Platform Dry Mass	282 kg	422 kg
System Margin	20%	
Satellite Dry Mass	**598 kg**	**733 kg**
Propellant Mass - Cold Gas	-	92 kg
Propellant Mass - Hydrazine	27 kg	253 kg
Adapter Mass (937 adaptor)	45 kg	
Launch Mass	**1748 kg**	
Launcher Allocation	*2100 kg*	
ΔV - Cold Gas		*> 50 m/s*
ΔV - Hydrazine	*> 90 m/s*	*> 590 m/s*

Fig 6.4-1 *On the left*: overall Dry Mass budget. *On the right*: total Mass end ΔV budget for the satellites at launch.

We arrive at **598** kg dry mass for the R. satellite and **733** kg for the F.A. satellite. The total mass with margin including propellants and adaptor, **1748** kg, fits well in the allocation mass of a Soyouz launcher [fig. 6.4-1].

	Receiver Satellite	F.A. Satellite
	Average Power Consumption	
Satellite Bus	300 W + 20%	300 W + 20%
Satellite Payload	200 W + 20%	250 W + 20%
System Margin	20%	
Satellite Power Consumption	720 W	790 W
Required from Solar Arrays (15° solar incidence)	745 W	820 W
EOL Power Available from Solar Arrays (15° solar incidence)	> 900 W @ 7 years with XTJ Cells > 20% SA Design Margin	> 900 W @ 7 years with XTJ Cells 10% SA Design Margin

Fig 6.4-2: Power resources needs for each spacecraft.

	Fresnel Array Satellite		Receiver Satellite
	Hydrazine Propulsion System **(m/s)**	Cold gas propulsion **(kg)**	Hydrazine Propulsion **(m/s)**
Orbit & FF Acquisition	50		50
Station Keeping	20		20
Mission - Reconfigurations	500	50	
Safe & RW Unloading	20		20
Total	**590**	**50**	**90**
Hypothesis	*Isp 220s, Thrust Efficiency 98%, Residuals 2%*	*Isp 65s, Thrust Efficiency 95%, Residuals 2%*	*Isp 220s, Thrust Efficiency 98%, Residuals 2%*

Fig 6.4-3: Propulsion ΔV Budget.

A fraction of cold gas is reserved for the fine pointing and attitude control.

6.5 Specific environmental constraints (EMC, temperature, cleanliness)

L2 is less radiation-bombarded than lower orbits. Temperature is not critical in UV. The membrane will eventually be hit by micrometeorites, the additional holes will contribute to order zero of diffraction, which is blocked. They will lessen the transmission in order +1 and add stray light. This has not been evaluated, but a solution exists in the unlikely case that the results of evaluation show an effect in 5 years: a double sheet membrane, the sheets being separated by a few millimetres. The probability of a double perforation oriented in the direction of the Receiver S/C being low, this cancels the effect of most perforations.

6.6 Special requirements

For security reasons, a minimum inter-satellite distance is to be respected. It is usually considered ~100m. With working distances of a few kilometres, we are in the safe range.

6.7 Current heritage and Technology Readiness Level (TRL)

Techno.	Actual developments	TRL	Improvements to be scheduled
General very fine FF-GNC softwares	Theoretical studies	03	Validate all the algorithms for very fine GNC servo-control loops.
closed loop FFRF hydrazine propu°	PRISMA proved rendezvous, reconfiguration, 8-km distance FF.	06	Controlling and stabilizing the formation sharply across huge distances (> 10 km)
RF sensing	Validated by PRISMA	07	
Propulsion: Cold gas, hydrazine	Flight proven on many satellites. (Ex: GRACE for cold gas)	09	
SSS	Flight proven	09	
Gyro120	Flight proven	09	
Reaction Wheels	Flight proven	09	
Nominal Platforms	PROTEUS flies	09	
Platform Adaptation	Theoretical studies	04	Adaptation for R. & F. A. S/C

6.8 Proposed procurement approach

The equipment proposed is mostly "off the shelf": stellar sensors, gyro, transmission, thrusters. They are all developed in Europe (ITAR-free).

6.9 Critical issues

Formation flying is usually considered critical. However, the precision requirements here are low. The highest precision required in this project concerns the attitude of the receiver spacecraft: 10^{-6} radians, and that is not a formation flying specificity

7. Science Operations and Archiving

7.1 Science Operations Architecture and proposed share of responsibilities

The platforms and telescope (including chromatic correction and field optics) are built by ESA. The instrumentation will be built by member states and data processing taken care of by consortium institutions. Negotiations are being started between scientists groups for this project. Terms are not yet defined, but the structure is getting ready to start if the proposal is accepted.

7.2 Archive approach

- On-board reconstruction of spectra and images, temporary storage.

- Ground based archive storage. Expected volume and format of the acquired data:

- In image mode, an image size will be 4000x4000 pixels, to obtain a correct oversampling of a 1000x1000 resel field. Each pixel will be digitized in 32 bits. So we arrive at **64 MBytes** per raw image.

- In spectro-imaging mode: each raw image are in 20 x 20 x 4000 cubes format. It occupies **6.4 MBytes** considering that spectral irradiance is digitized in 32 bits.

A compression ratio of 1:3 may be applied to retain only significant data.

7.3 Proprietary data policy

Data will be public as much as collaboration with other institutions makes it possible.

8. Technology development requirements

8.1 Payload technology challenges and technology development strategy

8.1.1 4-m size spreadable membrane and its deploying structure

A first concern is the manufacture of large Fresnel Array membranes then comes the folding issue. We prospect a 0.1-mm thick water-jet to cut out the patterns (the thinnest ones in the array corner are ~0.5 mm wide), with a precision that conforms to Δr constraint (~50 μm).

- ESA already leads R&T on membrane telescopes. A full scale spreadable membrane should be developed in phase A/B1: TRL04 by the end of 2012, TRL05 by the end of 2013.

- The deploying structure is already validated at TRL04 [cf. 5.10]. We expect to gain TRL05 at phase A/B1.

8.1.2 Blazed diffractive Mirrors (BDM) and UV coatings

TRL04 is expected by the end of 2011 (cf. challenges in § 5.10). In complement, an R&T CNES contract will be engaged in 2011 to perform the validation on a laboratory demonstrator. TRL05 is programmed by the end of 2013 as an outcome of phase A/B1.

8.2 Mission and Spacecraft technology challenges

- Verification of very fine GNC performances (ultimate angular precision: 8 mas).
- During phase A/B1, development and verification of the algorithms and software for the very fine Formation Flying Guidance Navigation & Control in L2 (ground and space segment).
- Platform adaptation for Receiver S/C: it should insure a 20 mas attitude stability and a reliable calibration closed loop with the ground. Moreover, the VANS needs to be integrated in the instrument itself while assuring the demanded performances.
- Platform adaptation for Fresnel Array S/C: the challenge is to develop adequate structures to receive a spreadable membrane and its sunshield.

9. Preliminary programmatics/Costs

9.1 Overall proposed mission management structure

A consortium could be formed with scientists from *Obervatoire Midi-Pyrénées*, *Observatoire de la Côte d'Azur*, *Universidad Complutense de Madrid*, NUVA, CfA, *Observatoire de Genève*.

9.2 Mission schedule drivers (technology developments, etc)

The schedule drivers are the readiness of the UV optics, normally tested in 2011, and the spreadable membrane under development.

9.3 Satellite/payload Cost

Satellite costs were thoroughly appraised by *Price Systems*: Tables 9.3-1 are given for a three channel 4-m FDAI scenario analysed at phase 0:

	COST (K€)
Total F.A. satellite + Formation Flying	**129 458**
Project Office	9 020
Engineering	28 881
PFs & Formation Flying validation	25 800
General Assembly Integration & Test	13 371
Ground Support Equipment	3 497
Products (contrators, componants...)	48 889

Element	COST (K€)
Total Receiver satellite	**176 237**
Project Office	13 291
Engineering	59 155
General Assembly Integration & Test	28 024
Ground Support Equipment	8 198
Products (contrators, componants...)	67 569

Table 9.3-1 Costs evaluation synthesis for a 3-channel 4-m FDAI (satellites including payload)

Amending this cost estimation makes 13000 K€ saved:

- With only two channels, 7000 K€ are saved (AIT + components)
- Additional 6000 K€ are saved if the component reliability is down casted from HI-REL to MIL, according with a 5-year lifetime mission.

Thus, for this 2-channel 4-m FDAI, we come to these satellites prices:

	F.A. satellite + Formation Flying	Receiver Satellite	TOTAL for satellites
Cost (K€)	**126 458**	**166 237**	**292 695**

9.4 Assumed share of payload costs to ESA

In the *Fresnel Array Satellite*: The spreadable Fresnel Array membrane, its unfolding structure and baffle.

In the *Receiver Satellite*: The field telescope, the Dic, the two chromatism correctors, the VANS (optics + sensors).

9.5 Estimated non-ESA payload costs

Member States will insure the development and costs of scientific instruments at focal plane: spectrographs, scientific cameras comprising their dedicated electronics.

9.6 Overall mission cost analysis

Total overall mission cost is optimised for a 4-m FDAI with 2 scientific channels [tab. 9.6-1]:

	Suggested share by ESA (K€)	Optimisation for 4-m FDAI (K€)
Total spacecraft activities	258 500	**292 695**
Launcher services	70 500	**74 305**
Ground Segment and Operations	94 000	**56 000**
ESA project	47 000	**47 000**
GRAND TOTAL	470 000	470 000

Table 9.6-1 Optimised overall costs for the 2-channel 4-m FDAI-UV

The assessed overall costs of the proposed mission match the budget of an ESA class M mission.

10. Communication and Outreach

Yes, the UV astronomy lacks communication. And, no, there is not yet a "killer science case" to propose for the UV, as far as we know, but this may well change. The problem with UV astronomy is that it is much less developed than radio, IR or visible, or even high energy photons. It cannot be done from the ground, and few missions have flown. So, little is known about the UV Universe, and many questions remain to be asked, before they are to be answered.

We propose to change that state of things, by providing beautiful images of galaxy centres and planetary systems in formation, by probing in a more complete way, many domains, from the high energy matter, to solar system borders, by asking new questions, and by answering them.

Our institutions are in close relation with science museums: in Barcelona, in Toulouse (cité de l'espace) and in Paris (Palais de la découverte - cité des sciences). Most of us are also science teachers. Our work with universities, colleges and high schools is of prime importance for science diffusion and public outreach, especially the young public, the future generation of scientists

11. Glossary

AGB: assymptotic giant branch (stars)

AGN : Active Galactic Nuclei

AIT: Assembly Integration & Test

APS: Active Pixel Sensor

AU: Astronomical Unit

BDM: Blazed Diffractive Mirror

COS: Cosmic Origins Spectrograph (instrument on the Hubble space telescope)

CTE: Thermal Expansion Coefficient

Dic: Dichroic Beamsplitter

EMC: Electro-Magnetic Compatibility

F. A. S/C: Fresnel Array S/C

FDAI : Fresnel Diffractive Array Imager

FF: Formation Flying

FFRF: Formation Flying Radio Frequency

FOG: Fiber Optics Gyro

FOV: Field Of View

FUSE: Far Ultraviolet Spectroscopic Explorer

FUV: Far UV

GNC: Guidance Navigation & Control

HST-GHRS ; HST-STIS :

I&T: Integration & Test

IFOV: Instantaneous Field Of View

IR : InfraRed

IRAP : Institut de Recherche en Astrophysique et Planétologie

ISL: Inter-Satellite Link

ISM: Inter-Stellar Medium

LGA: Low Gain Antenna

mas: milliarcsecond

MBA: Main Belt Asteroids

MGA: Medium Gain Antenna

MUSE: Multi-Unit Spectroscopic Explorer

NEA: Near Earth Asteroids

NUV: Near UV

NUVA: Network for UltraViolet Astronomy

pc: parsec

PMS: Pre-Main Sequence

PSF: Point Spread Function

QSO: Quasi stellar object (quasar)

resel: element of resolution ($\rho = \lambda / \phi_{aperture}$)

R. S/C: Receiver S/C

RFS: Radio Frequency Sensor

RIE: Reactive Ion Etching

RLOF: Roch Lobe OverFlow

RTRA-STAE: Réseau Thématique de Recherche Avancée / Sciences et Technologies pour l'Aéronautique et l'Espace (joint venture of public and private funds)

S/C: Spacecraft

SFD: Size Frequency Distribution

SN-: Super Novae

SPELTRA: Structure porteuse externe pour lancements multiples Ariane (for stacking satellites)

SSS: Standard Stellar Sensor

TAS: Thales Alenia Space

TNO: Trans-Neptunian Objects

UV : UltraViolet

VANS: Very Accurate Navigation Sensor

VIS: Visible

VLT: Very Large Telescope

WISE: Wide-field Infrared Survey Explorer (NASA satellite)

WR-: Wolf Rayet stars

WSO-UV : ? W S Observatory

YSO: Young Stellar Objects

12. References

We can provide videos of unfolding structures prototypes made by *BTS industrie*, and references on the companies that manufactures the optical technology for the optical testbeds. Follow the links put on the web page.

http://www.ast.obs-mip.fr/users/lkoechli/w3/index.html

Bibliography:

Atek, H., Kunth, D., Hayes, M., Östlin, G., Mas-Hesse, J. M. On the visibility of Lyman alpha emission in star forming galaxies: the role of dust, submitted to A&A, 2008.

de val Borro, M., Karovska, M. & Sasselov, D., 2009, ApJ, 700, 1148 Karovska et al. 2005, ApJ, 632, L137

Faklis D. & Morris M.G., "Broadband imaging with holographic lenses ", Optical Engineering, Vol. 28 No.6, p 592-598 (June 1989).

Gomez de Castro et al 2006; ApSS, 303, 33.

Hayes, M., Östlin, G., Mas-Hesse, J. M.,Kunth, D., Continuum Subtracting Lyman-Alpha Images: Low Redshift Studies Using the Solar Blind Channel of HST/ACS, submitted to AJ, 2007.

Herczeg et al 2004; ApJ, 607, 369.

Hinglais E., Phase 0 study on the "Fresnel Interferometric Imager" at C.N.E.S, Toulouse, France. Emmanuel Hinglais is responsible for this study carried out in 2008 and 2009.

Hyde R. A., "Eyeglass : Very Large Aperture Diffractive Telescopes" Applied Optics 38, No. 19, 4198-4212, (1 July 1999).

Karovska, M., Hack, W., Raymond, J., & Guinan, E. 1997, ApJ, 482, L175 Chugai, N.N., and Yungelson, L.R., 2004, Astron. Lett., 30, 65.

Karovska, M., Schlegel, E., Hack, W., Raymond, J. C., & Wood, B. E. 2005, ApJ, 623, L137.

Koechlin L., Serre D. Deba P. : Fresnel interferometric arrays for space-based imaging : testbed results, in "UV/Optical/IR Space Telescopes : Innovative Technologies and Concepts III", H. A. MacEwen J. B. Breckinridge Eds., SPIE Proc. Vol. 6687, San Diego, (August 2007).

Koechlin L., Serre D., Duchon P. "High resolution imaging with Fresnel interferometric arrays : suitability for exoplanet detection", Astronomy & Astrophysics vol. 443, 709-720 (2005).

Moos H.W. et al., Overview of the Far Ultraviolet Spectroscopic Explorer Mission, Astrophys. J. Letters, 538, L1-L6, 2000.

Morel S. and Koechlin L., "Recovery of moving objects from quantum limited data", Experimental Astronomy, 7, 117-127, (1997).

Östlin, G., Hayes, M., Kunth, D., Atek, H., Mas-Hesse, J. M., Leitherer, C., Petrosian, A., The Lyman alpha morphology of local starburst galaxies: release of calibrated images, submitted to AJ, 2008.

Schupmann L., "Die Medial Fernrohre : Eine neue Konstruktion for grosse astronomisch Instrumente" (B.G Teubner, Leipzig, 1899)

Sembach K.R. et al., The Deuterium-to-Hydrogen ratio in a low-metallicity cloud falling onto the Milky Way, Astrophys. J., Suppl. Ser., 150, 387-415, 2004.

Serre, D., Deba, P. Koechlin, L. : Fresnel Interferometric Imager : ground-based prototype, Applied Optics 48(15), pp. 2811–2820, (2009).

van Dishoeck et al 2006; Faraday Discussions, 133, 231.